Tectonophysics 793 (2020) 228596

Contents lists available at ScienceDirect

Tectonophysics

journal homepage: www.elsevier.com/locate/tecto

Seismic potential of the Dead Sea Fault in the northern Gulf of Aqaba-Elat: New evidence from liquefaction, seismic reflection, and paleoseismic data

Mor Kanari[a,*], Tina M. Niemi[b], Zvi Ben-Avraham[c], Uri Frieslander[d], Gideon Tibor[a], Beverly N. Goodman-Tchernov[e], Neta Wechsler[c], Abdelrahmen Abueladas[f], Abdallah Al-Zoubi[f], Uri Basson[g], Shmuel Marco[c]

[a] Department of Marine Geology and Geophysics, Israel Oceanographic and Limnological Research, Haifa 31080, Israel
[b] Department of Earth and Environmental Sciences, University of Missouri-Kansas City, Kansas City, MO, USA
[c] Department of Geophysics, Tel-Aviv University, Tel Aviv 6997801, Israel
[d] Geophysical Institute of Israel, Habbal Shem Tov 6, Lod 7019802, Israel
[e] Dr. Moses Strauss Department of Marine Geosciences, Charney School of Marine Sciences, University of Haifa, Mt. Carmel, Haifa 31905, Israel
[f] Faculty of Engineering, Surveying, and Geomatics, Al-Balqa' Applied University, Al-Salt 19117, Jordan
[g] GeoSense, P.O. Box 921, Even-Yehuda, Israel

ARTICLE INFO

Keywords:
Dead Sea Transform
Paleoseismology
Paleoliquefaction
Seismic reflection data
Historical earthquakes
Seismic hazard

ABSTRACT

The cities of Elat, Israel and neighboring Aqaba, Jordan are major economic, cultural, and seaport centers. They are located on the northern shore of the Gulf of Aqaba/Elat (GAE) directly on the Dead Sea Transform. Yet the precise location of the fault trace and its tectonic activity are lacking. The interpretation of seismic reflection profiles across the GAE beach and paleoseismic trench data located 2.2 km north of the shoreline provide evidence that the active offshore mapped Avrona Fault extends onland along the eastern side of the Elat Sabkha (mudflat), where three prominent fault strands crosscut the sedimentary fill. Mismatch of reflector geometry across the faults and flower structures indicate strike-slip faulting with a normal-slip component. Subsurface data from two trenching sites provide evidence for a minimum of two surface ruptures and two paleoliquefaction events. Faulting is constrained by radiocarbon dating for an Event 1 between 897 and 992 CE and Event 2 after 1294 CE. We suggest that the historically documented 1068 CE, and at least one later earthquake in 1458 or 1588 CE, ruptured the Elat Sabkha site. Based on fault mapping, we suggest a minimum value of M 6.6 for the 1068 CE earthquake. Whereas no surface rupture was observed for the 1212 CE historical earthquake, fluidized strata radiocarbon dated to before 1269–1389 CE identified as paleoliquefaction may be attributed to it. Two liquefaction sand-blows mapped in the trench likely formed after 1337 CE and before 1550 CE, which possibly occurred at the same time as in the second faulting event. Our data suggest that no large event occurred along the Avrona segment in the past ~430–550 years. Given a ~ 5 mm/yr slip rate, we conclude that a significant period of time passed since the last surface rupturing on the Avrona Fault, increasing its seismic potential.

1. Introduction

A key element of seismic hazard assessment is the characterization of seismogenic sources. The characterization of a seismic source involves detailed geologic and geophysical studies to exactly locate active faults and to determine the potential magnitude, rupture length, and recurrence of earthquakes on the fault. We investigate a strand of the Dead Sea Transform fault, known as the Avrona Fault, that has been mapped offshore in the Gulf of Aqaba/Elat (GAE) using seismic reflection data (Hartman et al., 2014, 2015) and to the north of the city using paleoseismic trenching (Amit et al., 1999, 2002). However, within the municipality of Elat, no active fault deformation or other evidence of past earthquakes has been previously documented.

The cities of Elat (Israel) and Aqaba (Jordan) are located at the north tip of the Gulf of Aqaba/Elat (the northeast extension of the Red Sea; Fig. 1). These cities are major economic, cultural, and recreational centers for southern Israel and Jordan, and vital aerial and marine ports. Both Elat and Aqaba are built on active plate boundary faults, which have ruptured in the past. Aqaba was completely destroyed in the 1068 CE earthquake (Ambraseys et al., 1994; Avner, 1993; Whitcomb, 1994; Guidoboni and Comastri, 2005; Ambraseys, 2009) and significant damage to structures in both Elat and Aqaba was

* Corresponding author.
E-mail address: mor.kanari@ocean.org.il (M. Kanari).

https://doi.org/10.1016/j.tecto.2020.228596
Received 12 March 2020; Received in revised form 12 August 2020; Accepted 19 August 2020
Available online 26 August 2020

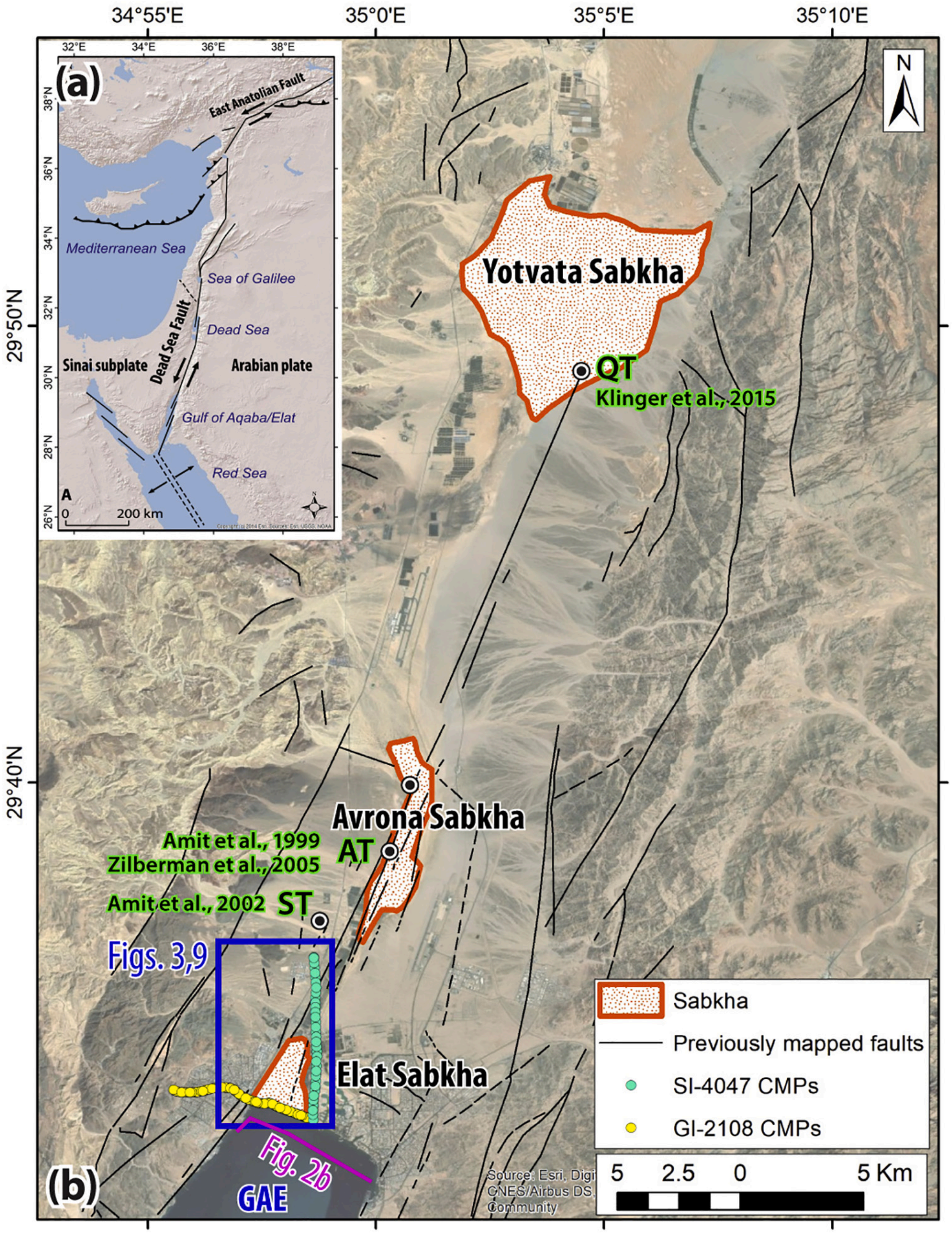

Fig. 1. (a) Regional tectonic map of the Dead Sea Transform and location of the Gulf of Aqaba/Elat; (b) Topographic image map of the southern Arava Valley showing location of the study area of the Elat Sabkha. Previously mapped faults in black lines (after Garfunkel, 1970; Garfunkel et al., 1981; Sneh et al., 1998). Previous study sites including Avrona Sabkha and Yovata Sabkha and locations of the paleoseismic trenches (in block circles): QT = Qatar trench (Klinger et al., 2015); AT = Avrona Trenches (Amit et al., 1999; Zilberman et al., 2005); ST = Shehoret trenches (e.g. Amit et al., 2002). GAE = Gulf of Aqaba/Elat. CMP shots discussed in this study from seismic lines SI-4047 and GI-2108 are plotted as light-blue dots and yellow dots, respectively. The blue rectangle marks the extent of the study area maps presented in Figs. 3 and 9. The pink line represents the location of the offshore high-resolution seismic profile by Hartman et al. (2014) detailed in Fig. 2b. (For interpretation of the references to colour in this figure legend, the reader is referred to the web version of this article.)

inflicted by the Mw 7.21995 Nuweiba earthquake even though the epicenter was located ~90 km to the south (Hofstetter, 2003). During that event, liquefaction occurred in the cities of Elat and Aqaba, both in artificial fillings and in natural sabkha and coastal deposits (Wust, 1997), and subsequent geotechnical studies showed that the coastal zone is susceptible to liquefying (Mansoor et al., 2004; Abueladas, 2014; Abueladas et al., 2020). Clearly, assessment of seismic hazard in these neighboring cities is vital. Aqaba and Elat are located on a transition zone between two structural realms at the southern part of the Dead Sea Fault system (DSF): the deep *en echelon* submarine basins of the Red Sea (Ben-Avraham, 1985) and the shallow continental basins of the Arava (ten Brink et al., 1999), localizing into a single fault strand farther northward. A report (Wieler et al., 2017) followed by a recent webpage created by the Geological Survey of Israel (https://www.gov.il/en/departments/general/high-resolution-mapping-eilat) details earthquake hazards and mapped active faults in the Elat region (including results from this current study).

We aim to identify and locate the active faults in the Elat/Aqaba region, and especially within the boundaries of Elat itself, and estimate their seismogenic potential for earthquake hazard assessment. Given these goals, we analyze previously unpublished seismic reflection profiles that were collected across and along the Elat Sabkha and provide evidence for the neotectonic history of faulting. We also report on the first paleoseismic investigations in the city of Elat, within the Elat Sabkha and provide evidence of paleoearthquake ground rupture and liquefaction. By correlating the recently mapped offshore Avrona Fault (Hartman et al., 2014) with the onshore fault in Elat from both paleoseismic trenching and seismic reflection profiling, the seismic hazard potential of these faults can be better characterized within the heavily urbanized Elat city and its very closely neighboring Aqaba city.

2. Study area

The Gulf of Aqaba/Elat (GAE) and the 160-km long Arava Valley (Wadi ‘Arabah) northeast of the cities of Elat and Aqaba formed along the Dead Sea Transform (DST) plate boundary that separates the Sinai

Table 1
Radiocarbon age determination of charcoal samples from trenches T1 and T3.

Unit ID	Sample ID	CAMS #	$\delta^{13}C$	Fraction modern	±	$D^{14}C$	±	^{14}C age	2σ Cal. Age
T1									
T1 Unit C	ET1 02	158882	−22.1	0.9178	0.0024	−82.2	2.4	690 ± 25	1269–1385 CE
T1 Unit C	ET1 02 – dup.	158861	−22.1	0.9197	0.0028	−80.3	2.8	675 ± 25	1275–1389 CE
T3 Fault									
U0	ET3 133	158889	−21.3	0.9243	0.0024	−75.7	2.4	635 ± 25	1286–1396 CE
U1	ET3 130	158886	−25	0.8764	0.0029	−123.6	2.9	1060 ± 30	897–1024 CE
U1	ET3 131	158887	−25	0.8719	0.0033	−128.1	3.3	1100 ± 35	782–1020 CE
U1	ET3 122	158883	−22.5	0.8944	0.0067	−105.6	6.7	900 ± 60	1023–1248 CE
U2	ET3 132	158888	−25	0.8530	0.0030	−147.0	3.0	1275 ± 30	661–800 CE
U4	ET3 121	158864	−23.2	0.8788	0.0024	−121.2	2.4	1040 ± 25	906–1029 CE
U5	ET3 120	158863	−9.4	0.8728	0.0026	−127.2	2.6	1095 ± 25	891–1012 CE
T3 Sandblow1 (SB1)									
L7	ET3 124	158885	−21.9	0.9244	0.0031	−75.6	3.1	630 ± 30	1287–1399 CE
L6	ET3 123	158884	−21.1	0.9215	0.0024	−78.5	2.4	655 ± 25	1281–1392 CE
T3 Sandblow2 (SB2)									
	ET3 134	158890	−21.2	0.9152	0.0031	−84.8	3.1	710 ± 30	1256–1385 CE
	ET3 135	158879	−25	0.6362	0.0028	−363.8	2.8	3635 ± 35	2133–1903 BCE

(1) 13C values are the assumed values according to Stuiver and Polach (Radiocarbon, v. 19, p.355, 1977) when given without decimal places. Values measured for the material itself are given with a single decimal place.
(2) The quoted age is in radiocarbon years using the Libby half life of 5568 years and following the conventions of Stuiver and Polach (ibid.).
(3) Radiocarbon concentration is given as fraction Modern, D14C, and conventional radiocarbon age.
(4) Sample preparation backgrounds have been subtracted, based on measurements of samples of 14C-free coal.

subplate from the Arabian plate (Fig. 1a). Quaternary slip rate estimates of the DST vary between 2 mm/yr and 10 mm/yr based on offset drainage systems along the Avrona and Arava fault segments (Zak and Freund, 1966; Garfunkel et al., 1981; Ginat et al., 1998; Klinger et al., 2000; Niemi et al., 2001). For details of different sources of data for these studies see Table 1 in Le Beon et al. (2008). Geophysical data indicate that the GAE developed from an *en echelon* array of three basins formed between left-stepping, strike-slip faults (Ben-Avraham et al., 1979; Ben-Avraham, 1985). Gravity data (ten Brink et al., 1999) indicate that the northernmost basin of the GAE, called the Elat Deep, extends on land beneath the Elat Sabkha and Avrona Playa. *En echelon* basins extend northward from the GAE into the Timna/Yovata/Taba Playa, the Dead Sea, and the Sea of Galilee (e.g. Garfunkel, 1981).

Previous studies of the submarine structure of the northern GAE suggest that slip on the eastern and western boundary faults is predominantly normal and that both faults are active (Ben-Avraham et al., 1979; Ben-Avraham, 1985; Ben-Avraham and Tibor, 1993). However, recent high-resolution seismic reflection and bathymetric data (Tibor et al., 2010; Hartman, 2012; Hartman et al., 2014, 2015) revealed a complex fault system across the shelf of the northern GAE with varying degrees of recent fault activity. The GAE shelf (Fig. 2) can be divided into three structural fault blocks (Tibor et al., 2010).

Based on high-resolution seismic reflection data, Makovsky et al. (2008) and Hartman et al. (2014) suggest that the recently active segment in the northern GAE is the Avrona Fault with a left-lateral, slip rate of 0.7 ± 0.3 mm/yr in the Late Pleistocene and 2.3–3.5 mm/yr during the Holocene. Two intrabasinal faults east of the Avrona Fault have been inactive for the last several tens of thousands of years (Fig. 2) and motion from these faults has likely transferred to the Avrona Fault (Hartman et al., 2014). Hartman et al. (2014) calculate a Holocene vertical slip rate of 1.0 ± 0.2 mm/yr for the Elat Fault and 0.4 ± 0.1 mm/yr for the Aqaba Fault. These authors suggest that the geometry, slip rates, and slip history of the faults on the shelf show the following: 1) during the Late Pleistocene, several intrabasinal faults became dominant across the basin, and 2) during the Holocene, the submarine Avrona Fault accommodates most of the strike-slip faulting in this transform plate boundary setting.

The Arava Valley (Wadi ‘Arabah), striking northeast from the GAE shoreline, is a structural and topographic valley delimited along much of its margins by normal faults (e.g. Garfunkel et al., 1981; Ibrahim, 1991; Rashdan, 1988). The valley is crossed by the active, NNE-striking Avrona Fault segment in the south and the Arava fault segments in the north along the DST (Garfunkel et al., 1981). The long-term slip rate of about 4.5 ± 1.5 mm/yr on the Arava fault is in agreement with geodetic estimates of the current horizontal plate motion along the DST suggested to be 3.7–7.5 mm/yr (Wdowinski et al., 2004; Ostrovsky, 2005; Le Beon et al., 2008).

The Elat fault system consists predominantly of normal faults that juxtapose Pleistocene alluvial fan sediments and Holocene deposits. Garfunkel (1970) traced a fault that he named the Elat Fault along the western Elat Sabkha and the western coast of the northern GAE and mapped a branch of that fault along a bathymetric escarpment in the GAE. Shaked et al. (2004, 2012) interpreted the submergence and burial of coral reefs and archaeological campsites along the western coastline of Elat as evidence of earthquakes and related tsunami sediment transport. One event ~2300 yr BP was corroborated by tsunami deposits along the northern portion of the GAE (Goodman Tchernov et al., 2016). Shaked et al. (2004, 2012) suggested that slip along a segment of the western boundary normal fault caused subsidence of 1.8 m in two earthquakes in the past 5000 yr BP.

Paleoseismic studies of the Avrona Fault some 15–25 km farther north revealed slip on normal faults across the valley fill (Gerson et al., 1993; Amit et al., 1995, 1996, 1999; Enzel et al., 1996; Porat et al., 1996, 1997; Shtivelman et al., 1998) and on the Avrona strike-slip fault (Amit et al., 2002; Zilberman et al., 2005). Additionally, a historical rupture on the Avrona Fault at the Avrona Sabkha site is attributed to the 1068 CE earthquake. Paleoseismic studies on the Avrona Fault at the south end of the Yotvata (Taba) Sabkha, about 30 km north of Aqaba, are reported by Allison (2013) and Klinger et al. (2015). Klinger et al. (2015) report two fault zones were observed in the trench about 10 m apart. They identified a conservative minimum of six paleoearthquakes. Radiocarbon dating indicated that the time window exposed in the trench extends from present to 4000 yr BP, with clustered seismic activity between the 7th and the 15th century, around 2000 yr BP and between 3000 yr BP and 4000 yr BP.

3. Data and methodology

3.1. Seismic reflection data from the Elat Sabkha

Seismic reflection data were collected in the Elat and Araba Valley region of southern Israel region in the late 1990s (Frieslander, 2000), of

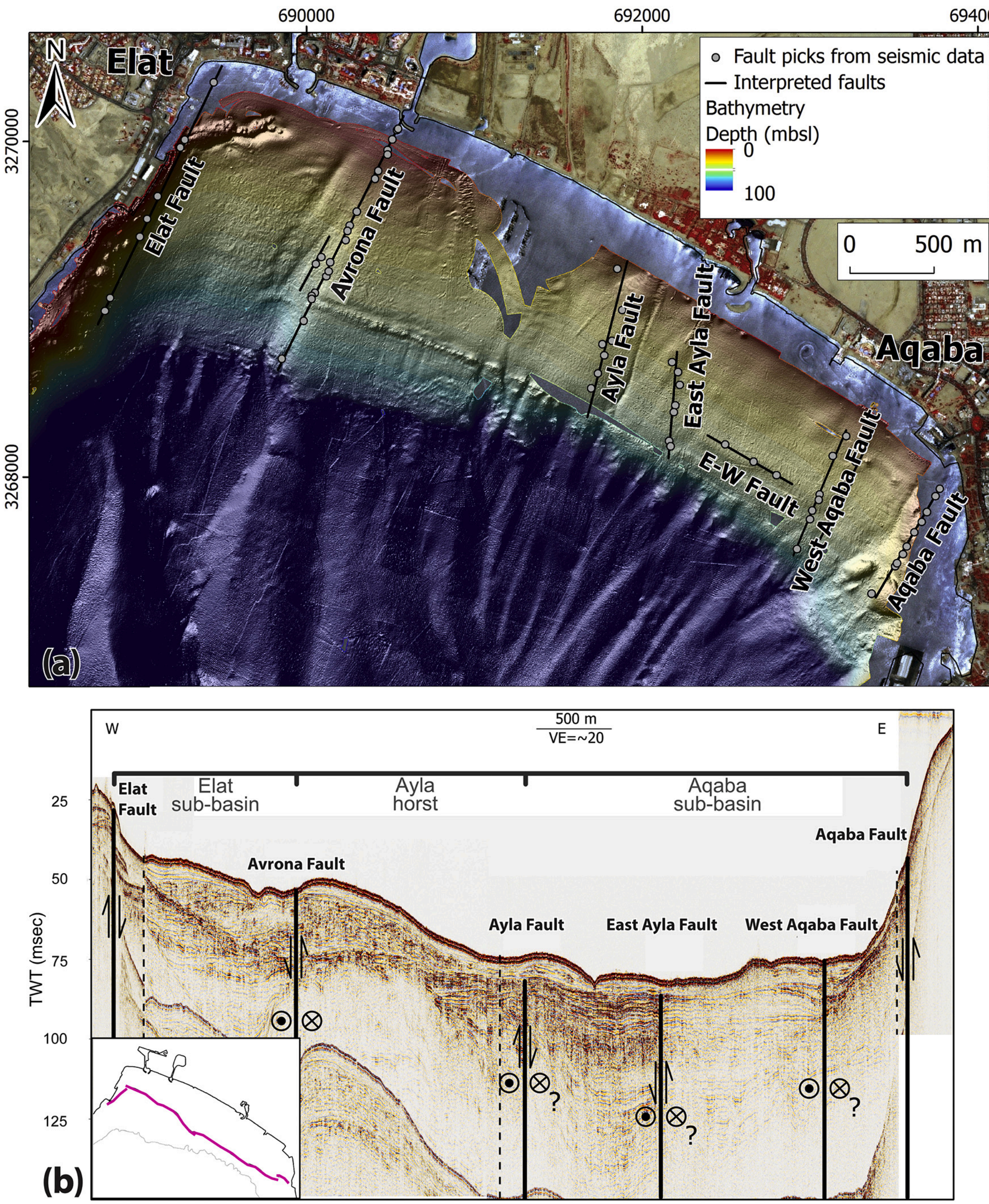

Fig. 2. (a) Bathymetric map of the north end of the Gulf of Aqaba/Elat (Sade et al., 2008; Tibor et al., 2010) showing the location of faults on the shelf of the northern Gulf of Aqaba/Elat as mapped from interpretation of seismic reflection data (Hartman et al., 2014). (b) A composite marine high-resolution seismic reflection profile across the gulf showing the six faults dividing the basin into the Elat sub-basin, Ayla horst, and Aqaba sub-basin (after Hartman et al., 2014). The location of the composite profile is marked in a pink line and the coastline of the GAE marked in black. (For interpretation of the references to colour in this figure legend, the reader is referred to the web version of this article.)

which three profiles are analyzed in this study (GI-2108, SI-4047, and GI-2210). The locations of the CMPs (Common Mid-Points) of the profiles in the study area are presented in Fig. 3, and the profiles presented in Fig. 4. The beach seismic reflection profile line (GI-2108) starts at the Elat Mountains to the west of the town and extends 5 km east-southeast along the beach (Figs. 1 and 3). The second line, SI 4047, was originally collected for oil exploration and later reprocessed by Frieslander (2000). Line SI-4047 extends from south at the shoreline to the north along a dirt round that parallels the international border between Israel and Jordan (Figs. 1 and 3). A third high-resolution profile, GI-2210, was collected parallel to the SI-4047 line across the fault zone.

Lines GI-2108 and GI-2210 were acquired using two Vibroseis vibrators with a 20 m VP (Vibration Point; center of the source vibrators array in the Half Integer Offset method) interval in a split spread array, yielding the VP in the center of each receiving station. A vibrator spacing of 10 m and move-up distance of 2.2 m were utilized. The sweep frequency was 18–120 Hz (linear) with 10 s length and 10 composites of sweeps per VP. The 120 receivers were 28 Hz geophones (1*6 inline) with a group interval of 20 m and split spread offsets of 0 m–50 m-1230 m for each 60 channels. Record length was 2 s with a 2 ms sample rate with a low cut at 20 Hz and a high cut at 175 Hz.

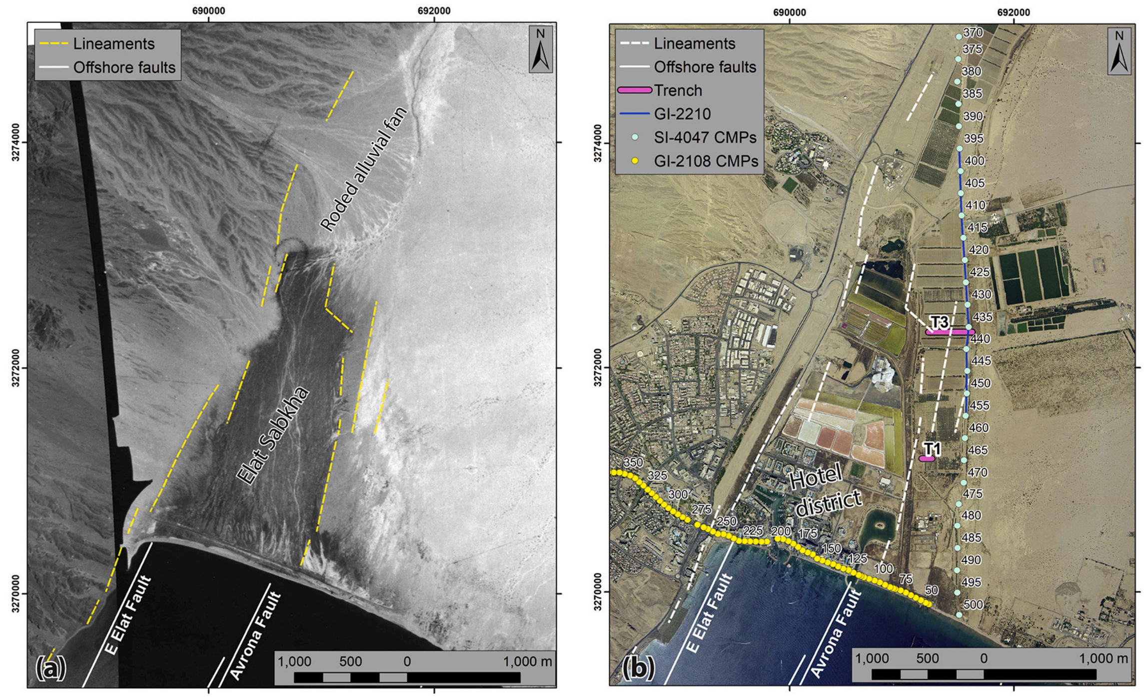

Fig. 3. (a) The trace of the East Elat Fault and the Avrona Fault offshore (white lines) as mapped from seismic reflection data (after Hartman et al., 2014), and interpreted lineaments suspect as fault traces around the Elat Sabkha (yellow dashed lines) based on a pre-urbanization aerial photo from 1945 (Palestine Survey PS43–6003 and PS43–6017). (b) The Avrona Fault offshore and the lineaments georeferenced to a modern satellite image, and the dataset used in the current study: location of seismic reflection profiles SI-4047 (light-blue circles mark CMP numbers), GI-2108 (yellow circles mark CMP numbers) and GI-2210 (blue line) and the paleoseismic trenches T1 and T3. The Hotel District of Elat is marked for reference to its vicinity to the surface rupture prone area. The seismic profiles are presented in Fig. 4. (For interpretation of the references to colour in this figure legend, the reader is referred to the web version of this article.)

The seismic reflection lines were processed utilizing gain, datum correction, predictive deconvolution, semblance CVS (Constant Velocity Stack) velocity analysis, auto statics, velocity analysis, NMO correction (Normal Move-Out), mute, stack, spectral balancing, time variant filter, AGC (Auto Gain Control), F-K coherency noise suppression (noise filterring in the Frequency-Wavenumber domain), and datum fix (Frieslander, 2000). The seismic velocity model for migrating the presented profiles was based on iterative analysis during the processing flows, which was matched with borehole velocity data from two boreholes tens of km farther north, which penetrated 1017 m of the Maastrichtian Ghareb Fm. down to the Early Cretaceous Hatira Fm., and 960 m of the Pliocene Takia Fm. down to the Early Cretaceous Hatira Fm. Borehole velocity data were available down to 395 m and 564 m depths. Estimated velocities were 2000 m/s for the top 0–0.4 s two-way travel time (TWTT), and 2400 m/s for the bottom parts below 0.4 s TWTT (Frieslander, 2000).

The seismic reflection profiles, which were originally located using the 1923 Cassini-Soldner Palestine projection of the old Israel Grid coordinate system, are transformed into UTM coordinates. Since both line localities were collected in different surveys and the SI-4047 line reprocessed, they required different geometric corrections. Analyses of the Line GI-2108 position data indicated the need for a 200 m translation to match the coastline road on which it was acquired. A 50 m translation was required to fix the SI-4047 (and GI-2210) line to the dirt road along the Israel-Jordan border. With these corrections, we were able to place seismic reflection lines in their proper geographic locations.

3.2. Paleoseismic trenching

Aerial photos from the 1945 PS (Palestine Survey PS43-6003 and PS43-6017) at a scale of 1:50,000 were used to map lineaments that are potentially locations of active fault surface rupture (Fig. 3). Lineaments on the 1945 air photo were based on colour, textural, and tonal differences. These interpretations were saved as a lineament file and projected onto the high resolution orthophoto of the city provided by the Elat municipality.

Based on the interpretation of aerial photos (Fig. 3) and the onshore projection of the submarine Avrona Fault as mapped from marine seismic reflection data (Hartman et al., 2014), a 90-m-long paleoseismic trench, T1, was excavated on the palm orchards of Kibbutz Eilot, about 1 km north of the Elat shoreline (Fig. 3b). Trench T1 revealed liquefaction features, but the fault trace itself was not found. We then excavated a 70-m-long trench, T2, approximately 600 m farther north of T1, but this trench was quickly abandoned without further study due to a very shallow ground water table only 20–30 cm below the ground surface. A third trench, T3, was excavated 1200 m farther north from T1 (2.2 km from the shoreline) in an agricultural field. Trench T3 was 300 m long, and at the western part of it, the active trace of the Avrona Fault was found and documented (Fig. 5). The depth of the trench was limited to 1.1 m to 1.2 m because of the shallow water table. The trenches were excavated using a backhoe and their walls were cleaned, photographed, and logged using standard paleoseismologic methods (e.g. McCalpin, 2009).

4. Results

4.1. Seismic reflection profiles in Elat

Along line GI-2108, the Elat Sabkha is seen on the east side of the line as a basin filled with sediment to the bottom of the profile. Frieslander (2000) reports that the Elat basin has a sediment thickness of ~2 km of sediment. The Avrona Fault (CMP 125; Fig. 4a) is evident as a prominent narrow discontinuity that crosses the predominantly parallel reflectors of the Elat basin in a very localized band of deformation. The main trace of the fault is vertical with subparallel splay

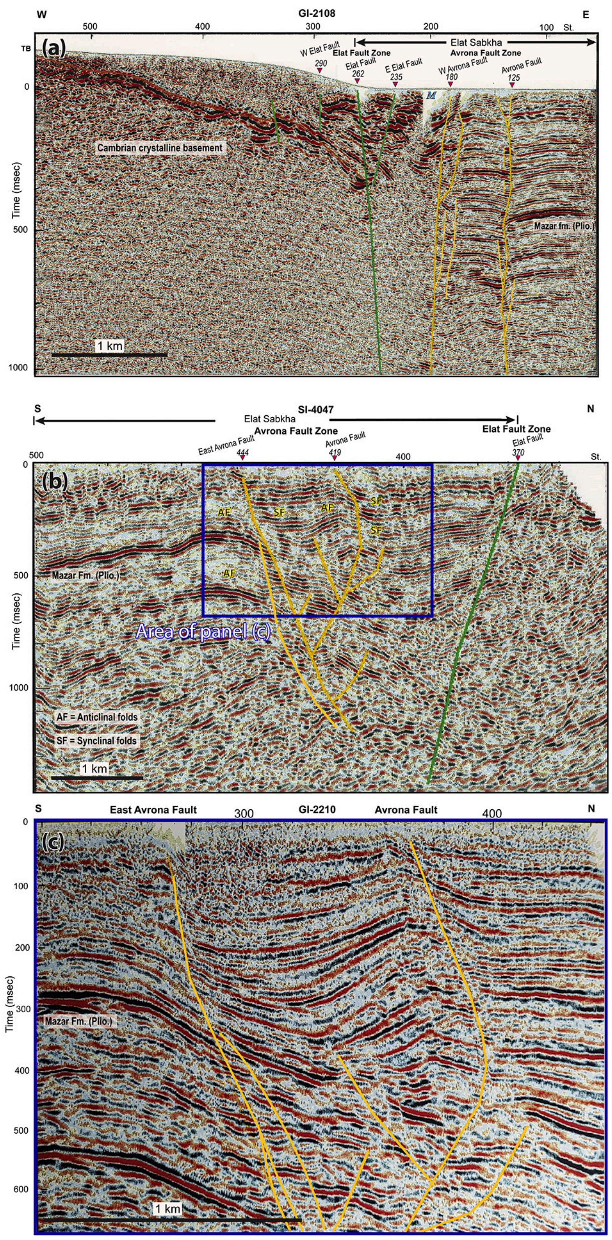

Fig. 4. (a) Seismic line GI-2108 extending E-W on the southern part of the Elat Sabkha including interpretation of the Avrona Fault strands (yellow) and the Elat Fault (green); specific CMP points at interpreted fault strands are marked in red triangles (same CMPs are marked in Fig. 9). (b) Seismic line SI-4047 extending S−N on the eastern part of the Elat Sabkha including interpretation of the Avrona Fault strands (yellow) and the Elat Fault (green); specific CMP points at interpreted fault strands are marked in red triangles (same CMPs are marked in Fig. 9). AF = Anticlinal Folds; SF = Synclinal Folds. (c) High-resolution seismic line GI-2210 extending S−N on the eastern part of the Elat Sabkha including interpretation of the Avrona Fault strands (yellow); This line overlaps line SI-4047 (panel b) while the high resolution allows to identify fault offsets and deformation reaching up close to the surface. See Fig. 3 for location of the lines. (For interpretation of the references to colour in this figure legend, the reader is referred to the web version of this article.)

faults which bend, branch upwards, and terminate. Close to the ground surface, the fault appears to branch upward into two or more strands. The parameters of the seismic data preclude imaging of the shallow (10s m) subsurface. We map the upward continuation of the fault to ground surface at CMP 125 in Fig. 4.

The Avrona Fault cuts predominantly parallel reflectors interpreted as sedimentary fill including aeolian, sabkha, fluvial, and marine deposits of the Elat basin. The seismic reflector pattern, the amplitude, the thickness between prominent reflectors, and the character of the reflectors are very different across the fault. Structurally, the beds on either side of the fault have apparent dips toward the fault, or are warped downward at the fault trace. The mismatch of the seismic stratigraphic sequences and dip directions across the fault indicate that it is a strike-slip fault. The Avrona Fault at CMP 125 aligns with the Avrona Fault mapped from Sparker seismic reflection data offshore (Hartman et al., 2014). The fault cuts through the basin fill indicating it is younger than the fault geometry that created the basin and suggests a youthful age of this fault location.

The West Avrona Fault in Line GI-2108, mapped at CMP 180 (Fig. 4a), contains several parallel and branching fault strands and separates the predominantly flat-lying reflectors of the Elat basin to the east from a series of discontinuous strong reflector sequences in the shallow subsurface. The high seismic impedance at the upper sequence west of the fault prevents deeper seismic penetration, which could result from the presence of salts, buried coral reefs, boulder conglomerates, or other lithologies. Although the reflectors are very discontinuous, the geometry of the upper 250 ms may roughly define a syncline west of the faulting. The lower sequence is predominantly seismically transparent and there is also a gap in the data acquisition due to the Elat marina (Marked as “M” on the seismic line in Fig. 4a) which obscures reflector geometry. Because of the strong mismatch of the reflector types in the top 200–300 ms across the fault, it appears that the West Avrona Fault is likely a strike-slip fault, possibly older than the Avrona Fault, since it appears to have little to no correlation between the two offset sides (the two sides of the fault), while the Avrona Fault appears to offset strata within the Elat Basin. It is difficult to discern if the fault extends to the surface, which would confirm recent activity, but it seems likely. From the interpretation of numerous marine seismic reflection lines by Hartman et al. (2014), no faults were mapped in the offshore across the location of CMP 180. Potentially, this may be because the West Avrona Fault does not offset the upper 75 ms penetrated by the Sparker seismic reflection data in the offshore (Hartman et al., 2014).

The strong reflectors at a shallow depth on the west side of line GI-2108 from CMPs 500–300 (Fig. 4a) represent the depth to Cambrian crystalline basement rock (Frieslander, 2000). These reflectors dip toward the east and are overlain by sedimentary units that are seismically transparent. The sedimentary cover above the basement reflector thickens toward the east. The normal faulting of the basement and the western boundary of the Elat basin is accommodated by the Elat Fault zone (green faults in Fig. 4a). At CMPs 290, the basement reflectors are offset about 100 ms by a down-to-the-east, normal fault. On this fault block above the basement is a series of east-dipping parallel reflectors which are overlain by onlapping reflectors with high reflectance. This geometry suggests an angular unconformity. The main Elat Fault is interpreted at CMP 262 as a steep plane that separates the basement from the thick sedimentary basin. The upper seismic section east of the main fault is characterized by a series of strong reflector packages that are discontinuous and offset across the Elat Fault and East Elat Fault at CMP 235. The East Elat Fault is the on-land continuation of the offshore Elat Fault mapped by Hartman et al. (2014). Basement was not imaged east of the Elat Fault, however, vertical slip on the fault is likely > 1.5 km based on gravity data (ten Brink et al., 1999).

Seismic reflection line SI-4047 crosses the east side of the Elat Sabkha from north to south (Fig. 4b). At CMP 370, the basin-bounding Elat Fault appears to separate parallel reflectors of the basin to the south from high reflectance horizons, presumably of the basement and sedimentary rocks. The upper 200–300 ms west of the Elat Fault zone contain some discontinuous parallel and wavy reflectors that likely represent sedimentary rocks and sediment cover. South and east of the Elat Fault, the upper 500 ms shows parallel reflectors that apparently dip predominantly to the south. The lower sections show folded and faulted strata. The Avrona Fault zone was interpreted on line SI-4047

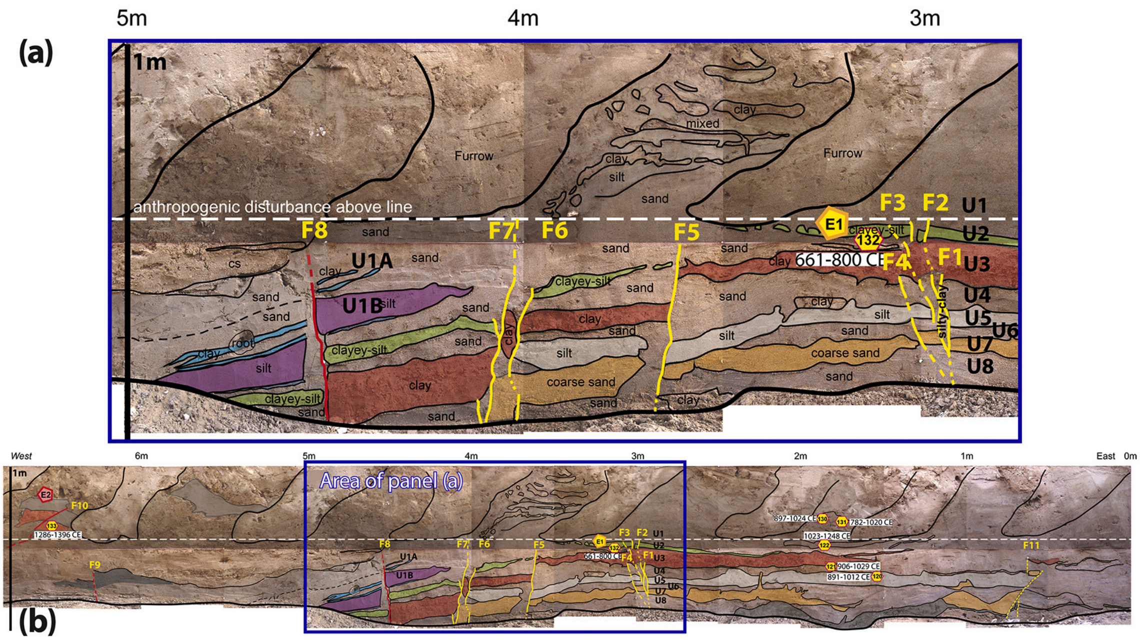

Fig. 5. Trench T3 log of the fault zone: The top 80 cm of the trench were disturbed by farming (marked by white dashed boundary). U1-U8 are stratigraphic units and F1-F11 are interpreted fault strands (see text for detail). Yellow hexagons mark charcoal samples locations; dated samples have adjacent radiocarbon age determinations presented. E1 and E2 are the interpreted event horizons which represent the faulting events (see text for detail). (a) detailed blow-up of the 3–5 m faulted strata in the fault zone. (b) The complete 0–7 m fault zone log; blue rectangle marks the area of panel (a); The presented log is simplified for clarity of the figure; a high-resolution more detailed log is available in the supplementary material SM1. (For interpretation of the references to colour in this figure legend, the reader is referred to the web version of this article.)

with two strands at CMPs 419 and 444 that likely branch upward from one fault at a depth of approximately 1000 ms. Both faults have anticlinal folds on the south side and synclinal folds and offset strata on the north side of each fault. The structure at 419 forms a positive flower structure with reflectors dipping away from the main fault trace and multiple upward branching fault splays. The flower structure indicates that this is a strike-slip fault. The reflector geometry between the Elat Fault (CMP 370) and CMP 444 forms an overall structure of a syncline, with the strike-slip fault at CMP 419 cutting through the middle, which suggests this is a young structure. Finer details of the fault zone are shown on seismic reflection line GI-2210 (Fig. 4c). An apparently south-dipping, half-graben with growth strata thickening to the south (or southwest/southeast) can be seen between the two strike-slip faults in the upper 300–400 ms. This suggests a change in the style of deformation in the basin. The southern fault at CMP 275 (left-hand side of profile) on GI-2210 has a relatively simple structure without multiple upward branching fault splays. The fault appears to have apparent vertical separation down-to-the-northwest. It is likely a subparallel, left-oblique, normal-slip fault strand and may bound older units from the younger depocenter. South of the fault at CMP 444 on SI-4047 (Fig. 4b), the lower section between 500 and 1200 ms generally has apparent dips to the south with slightly steeper dips than the section above. Beds thicken toward the sea, indicating syntectonic sedimentation into a localized depocenter.

A prominent strong reflector package at the south end of line SI-4047 at 500 ms depth (Fig. 4b) correlates with the same strong reflectors on the east side of line GI-2108 at 400–500 ms (Fig. 4a). Frieslander (2000) suggested that this reflector package correlates to the Pliocene-aged Mazar Formation which is carbonate shale or marl. On line SI-4047, we see that the Mazar Fm dips from 300 ms at CMP 444 to 500 ms at the end of the line at CMP 500. Because the reflectors at 500 ms on line GI-2108 are flat, we can deduce that the seismic line is parallel to strike and the beds are dipping southwest.

In summary, the seismic data shows that the onland Avrona Fault zone crosses the Elat Sabkha striking ~020° and is approximately 750 m wide. The Avrona Fault, West Avrona Fault and East Avrona Fault offset the sedimentary fill of the Elat basin that underlies the Elat Sabkha. The main Avrona Fault is the continuation of the fault mapped offshore and extends from CMP 125 on line GI-2108 to CMP 419 on line SI-4047. The main Avrona Fault is a fairly simple strand at the coast (GI-2108) and is the main strand at the center of a positive flower structure about 3 km inland (SI-4047). The surface expression of the West Avrona Fault and its northeast extension are unknown, likely due to fluvial erosion of the Arava drainage. The East Avrona Fault is a single, simple fault strand that branches from the Avrona Fault at depth and is subparallel to it. Folding observed in seismic profiles is likely the result of the interaction of right- and left-stepping fault strand geometries across the sabkha. The southern portion of the Elat Sabkha is dipping toward the southwest with syntectonic deposition and thickening of strata to the southwest (Fig. 2). The Elat Fault Zone (green faults in Fig. 4) along the western boundary of the Elat Sabkha has several normal fault strands, of which the easternmost (East Elat Fault) apparently correlate to the active offshore fault and bathymetric escarpment discussed by Hartman et al. (2014).

4.2. Paleoseismic evidence

4.2.1. Paleoearthquake surface rupture

Interpretation of the 1945 aerial photographs indicates that the Elat Sabkha is a coastal mudflat that extends from the shoreline to approximately 2.8 km inland where it appears to border the Roded alluvial fan and probably interfingers with it in the subsurface (Fig. 3). The sabkha developed along the outlet of the SSW-draining Arava valley where it empties into the Gulf of Aqaba/Elat. In the 1945 aerial photo, multiple anastomosing to gently meandering channels can be seen crossing the sabkha (Fig. 3a). Today, these channels collect into one canal to the east of the main hotel district (around CMP 75 of line GI-2108 in Fig. 3b). The margins of the sabkha are marked by distinct, NE-trending lineaments (marked in yellow in Fig. 3a). The westernmost lineament appears to be the boundary between older and younger alluvial fans previously identified as the location of the Elat Fault (e.g. Garfunkel et al., 1981; Gerson et al., 1993). On the eastern side of the sabkha are three subparallel lineaments marking the boundary between different zones of the sabkha based on their appearance (colour and texture) in the aerial photo. We interpret the eastern border of the Elat Sabkha as the location of the Avrona Fault zone as was also suggested by previous authors (e.g. Garfunkel, 1970; Garfunkel et al., 1981; Amit et al., 2002). We excavated our trenches T1 and T3 there (pink lines in Fig. 3b).

The sediment exposed in Trench T3 shows a sequence of shallow, sand-filled channels and overbank floodplain and mudflat deposition (Fig. 5). Laterally migrating and gently aggrading channel fill is typical for the eastern portion of the trench. The channels are approximately 2 m wide and 30 cm deep. They are filled with predominantly fine- to medium-grained sand with cross-bedding that indicates east-west oscillations of the channel's margins. Point bar cross-beds are often draped by mud at their tops suggesting an original depositional dip for some fine-grained units in the trench. The western portion of the trench is dominated by interbedded sand, silt, and clay layers interpreted as flooding events. Beds of laminated mud and silt suggest periods of standing water. The uppermost 80 cm were anthropogenically disturbed due to deep agricultural plowing (Fig. 5).

The fault zone in Trench T3 is 9 m wide and consists of eleven fault strands that terminate upward at different stratigraphic levels that suggest two possible surface rupturing events. Fault F11 is the easternmost fault. Faults F1-F4 are a series of upward-branching strands of one fault trace with very little observed vertical displacement of up to 1.5 cm and a slight push-up geometry. Fault F11 is insufficiently mapped due to the lack of fine-grained interbeds to provide much detailed history of faulting at this location. F5 and the combined F6/F7 have normal components across them with down-to-the-west offset of apparent 10 cm and up to 15 cm, respectively. F8 has 12 cm of down-to-the west, apparent vertical separation. Total apparent vertical separation across F3 to west of F8 is 43 cm measured for the change of elevation of clayey silt layer U2. F9 shows apparent vertical offset of 7 cm down-to-the-west at the top of a silty-sand layer, but the trench floor interferes with tracing it further down. F10 is above the anthropogenic disturbance zone and thus has significant uncertainty in its mapping and interpretation. There is apparent vertical change on both sides of F11, but with insufficient evidence to identify the faulting history. If the original topography of the ground prior to faulting had a ridge and swale morphology as is common in a fluvial environment, then lateral slip on faults would cause apparent vertical separation of stratigraphic units. Furthermore, if there are rapid lateral changes in stratigraphic thickness of units in the depositional environment, then strike-slip on a fault would also cause apparent vertical offsets. Because the apparent offsets are all down-to-the west (except F11), this could indicate that there is a component of normal slip on the faults.

Below the anthropogenic disturbance (plow zone), we define eight marker layers (units U1-U8) across the faulted portion of the trench (Fig. 5). Layer thickness of units varies across the fault traces. This is especially true for Units U3 and U4. U5 has distinct notable variation in thickness across this strand. Furthermore, mismatch of layer thickness across the fault strands suggests strike-slip fault motion as would be expected for the Avrona Fault. The layered stratigraphy in the upper interfurrow segment suggests that F5 fault rupture terminates in unit U1. Given what we can discern from the overlying stratigraphy within the interfurrows, we posit that faults F1-F7 offset units U2-U8 in an event labeled E1. Faults F11 and F1–7 appear to terminate in the sand of U1 below or near the anthropogenic disturbance zone. These data indicate a possible surface rupture event after the deposition of U2 and before deposition of the silt layer in the U1 sand layer (Fig. 5). As the silt layer in U1 (radiocarbon sample ET3–122 dated at with a 2-sigma calibrated age of 1023–1248 CE) does not directly cap the faults, but is the uppermost last continuous unit below the anthropogenic disturbance zone, we have utilized this as the post-event horizon. However, radiocarbon analyses of samples 130 and 131 that are stratigraphically above this layer, within the zone between furrows, were used in the age model as described below.

Stratigraphically above the Units U1-U8 and to the west are younger layers of the sabkha (Fig. 5). Units U1B (silt) and U1A (clay) were deposited above the U1 sediment. These units and older U1-U8 units appear to dip gently to the west. Given the appearance of the dipping clay strata on the migrating channel deposits exposed to the east and the sedimentary contact to migrating point bar sequence in a channel, we interpret the dip of these layers to be tectonic. Within a predominantly flat-lying, aggrading depositional environment, the approximate 5–10 degree dips indicate tectonic tilting or folding. The dipping units appear west of F5, F6/7, and F8. U1B and U1A have an apparent vertical offset of 12 cm across F8. It is not clear whether the silt and clay layers above F5-F7 in the interfurrow area is equivalent to U1B and U1A. If they are, then F6–7 likely extends higher in the stratigraphic section and would post-date motion on F5 (E1). The upper termination of F8 is not known because of the deep plowing. However, based on the given data, it appears that F8 cuts higher in the stratigraphic section than F1-F5. Faults F9-F10 offset Units 1B and 1A and sand, silt, and clay layers that are stratigraphically younger. We do not have any stratigraphic control of the capping layer of this proposed event (E2).

Given the limitation of the dataset due to anthropogenic modification of the site, we interpret at least two fault ruptures in Trench T3. We interpret the trench data as: (1) the first event (E1) ruptures units U2-U8 (F1-F5, and possibly F11), (2) deposition of units U1B and U1A and overlying layers in the accommodation space created by down-to-the-west faulting; (3) second event (E2) on F6/F7 and/or F8-F10.

4.2.2. Paleoliquefation

The size, frequency, and distance from an epicenter of earthquake-induced liquefaction features depend largely on the strength of the ground motion, a high water table, and the presence of soil susceptible to liquefy (e.g. Tuttle et al., 2019). The 1995 rupture of a submarine fault of the DST system in the Gulf of Elat/Aqaba in the Mw 7.2–7.3 Nuweiba earthquake (Dziewonski et al., 1997; Hofstetter, 2003) about 90 km southwest of Elat created liquefaction sand blows in the city (Wust, 1997). These sandblows are still visible on the ground surface (Fig. 6). In this study, we document evidence for paleoliquefaction in our trench exposures.

Two liquefaction structures (Fig. 6a, b), rather large in size (up to 5 m in diameter and 1 m high) were documented in Trench T3 west of the location of the fault rupture. A representative section of the stratigraphy composed of 7 main units (L1-L7) is presented in the log (Fig. 6a). A large liquefaction sand blow (SB1) is mapped as a mound of unstratified sand which seems to have torn through and carried some of the silt, clay and clayey silt layers as rip-up clasts within the sand and has deposited these layers away from the center of the feature. The boundaries of SB1 are outlined in black dashed rectangle in Fig. 6a. Layer (L3) caps the SB1 liquefaction feature. Sand blow 2 (SB2) has a similar construction with a mound of unstratified sand flanked by fine-grained sediment sloping away from the vent (Fig. 6b). The feeder dikes for each of these features was not identified. We interpret this as evidence for liquefaction at shallow depth and not a deep-sourced injection type. Radiocarbon samples within the sand blow provide a minimum age of formation of ~400 years BP as detailed below.

Trench T1 (Fig. 6) revealed liquefaction deformation features but no fault trace was evident. The uppermost unit A is disrupted by modern agriculture similar to the plow furrows observed in Trench T3. Below Unit A is a sand unit (Unit B; no sharp boundary or difference between them but the disrupted soil in unit A) and a laminated unit of alternating silt and clay (Unit C). Unit D contains interbedded layers of medium-grained sand with ripple laminations, coarse sand lenses, and very fine sand. Clear evidence of fluid escape structures is evident (Fig. 6c). This includes contorted and disrupted beds and ball-and-pillar

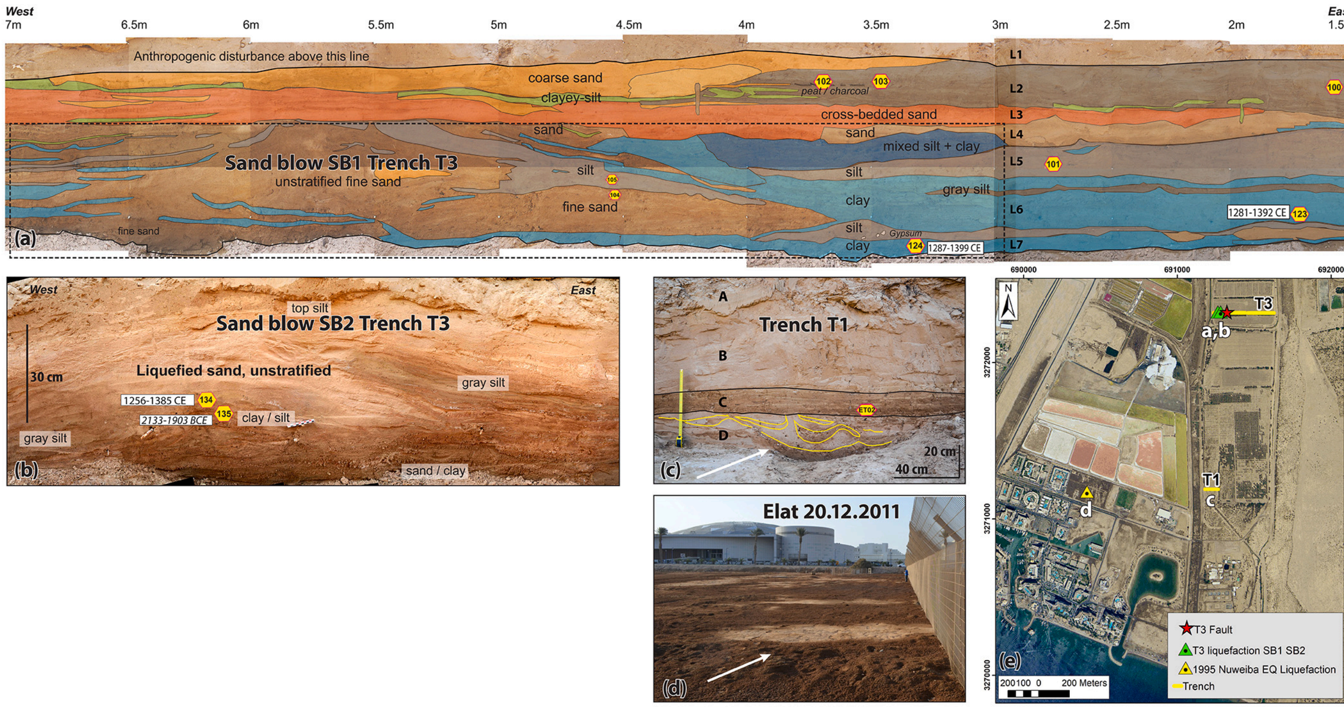

Fig. 6. Liquefaction features and their spatial extent. (a) Trench log of Sand blow 1 structure (SB1) in T3 and its logged stratigraphic structure; boundaries of sand blow outlined in black dashed rectangle; L1-L7 are stratigraphic units of the West Sabkha (see text for detail). Yellow hexagons mark charcoal samples locations; dated samples have adjacent radiocarbon age determinations presented. (b) photo mosaic of Sand blow 2 structure (SB2) in T3; no detailed log is available for SB2. (c) T1 liquefaction fluid escape structures (interpreted in yellow on photo) and its charcoal ET02 sample; white arrow points out liquefaction related feature. (d) liquefaction evidence from the 1995 Nuweiba M7.2 earthquake, still visible today in the vicinity of T1; white arrow points out liquefaction related feature; photo taken in December 2011; (e) map of trenches T1 and T3 area detailing the locations of all other features in the figure (panels a-d). For the reader's convenience, a high-resolution version of the figure is available in the supplementary material SM2. (For interpretation of the references to colour in this figure legend, the reader is referred to the web version of this article.)

structures in Unit D. This layer is capped by the flat-lying Unit C layer. Radiocarbon dating of unit C provides a maximum age for the interpreted liquefaction feature.

4.2.3. Radiocarbon dating and age models

A total of 12 charcoal samples were collected from Trench 1 and Trench 3 and were sent for radiocarbon analyses (Table 1). Radiocarbon ages were corrected for isotope fractionation and calibrated using the Calib 7.1 software (Stuiver et al., 2019). A sediment accumulation rate was calculated for deposits in Trench 3 at the fault zone and in the west sabkha near the sand blow locations (Fig. 7). Using the depth and ages of three lower radiocarbon results at the fault zone, a sedimentation rate of 0.9 mm/yr was calculated. At the location of the sand blow, using the depth and ages of the lower two radiocarbon samples yielded a 1.7 mm/yr sediment accumulation rate. These data suggest that subsidence and accommodation space within the Avrona Sabkha and fault zone varies by a factor of about two.

Age modeling using the OxCal program and the IntCal13 calibration curve (Bronk Ramsey, 2017; Reimer et al., 2013) was performed for the radiocarbon results and combined with stratigraphic data from the faulted section of T3. Units U8-U2 were deposited before an earthquake that appears to be capped by layers in the lower unit U1. Radiocarbon samples ET3–120 (U5), ET3–121 (U4), ET3–132 (U2) are below the event and ET3–122, ET3–131, ET3–130, and ET3–133 are above it (Fig. 5). Reiterative OxCal model runs for the above sequence identified three samples in poor agreement that were removed. The final OxCal age model included samples ET3–120, ET3–130, ET3–131, and ET3–133 as presented in Fig. 8. The 2-sigma age model result indicates that the first faulting event (E1) occurred between 897 and 992 CE, and the second faulting event (E2) occurred after 1287 CE. The agricultural plowing of the top of the trench prevents the dating of the cap. The historical records rule out significant earthquake surface ruptures in this location in the past ~450 years (e.g. Klinger et al., 2015).

Two liquefaction features at the same stratigraphic level were documented in the western portion of Trench T3 (Fig. 6). These features are interpreted to be earthquake-induced liquefied sand. The features are capped by flat-lying strata that lack radiocarbon age dating. One radiocarbon sample (ET3–135) yielded an age of 2133–1903 BCE. We suspect it is a remobilization of charcoal older than all other C-14 results for this trench. The process of liquefaction can fluidize saturated sands at depth and inject these to the surface. Three radiocarbon samples (ET3–124, ET3–123, and ET3–134) were collected from under and within the sand blows and thus pre-date the causative earthquake. Utilizing these ages below a boundary event in the OxCal modeling program indicated that ET3–134 was in poor agreement, and it was removed from the model. With the remaining two radiocarbon dates, a probability distribution for the age of liquefaction of 1294–1635 CE was obtained. If we use the sediment accumulation rate of 1.7 mm/yr and the depth to the capping horizon of 70 cm, then the capping layer (L3) began forming approximately 400 years ago. This would suggest that the sand blow formed before 1550 CE.

In Trench T1 (Fig. 6), a dewatering structure that is likely due to seismically-induced liquefaction is capped by laminated sediment of Layer C. The charcoal sample from this layer (ET02) yielded split sample radiocarbon ages of 690 ± 25 and 675 ± 25 (Table 1). The calendar age range for these two samples is 1269–1389 CE indicating that the liquefaction event occurred sometime before the late 13th to late 14th centuries.

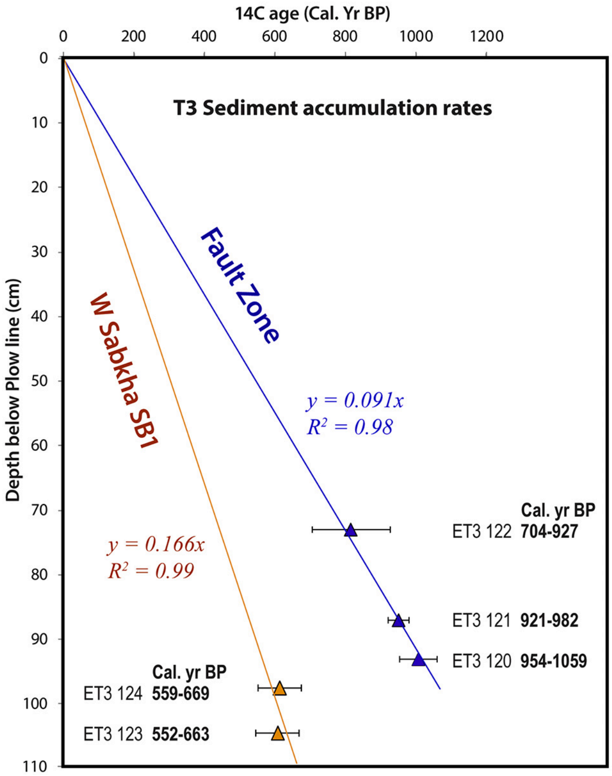

Fig. 7. Sediment accumulation rate estimation for trench T3: using the calibrated year BP ages of the radiocarbon ages from the bottom of the trench and the measured depth to the top of the trench, an accumulation rate was calculated. The triangles are radiocarbon ages with 2-sigma error bars and the solid lines are the linear interpolation regressions. The fault zone ages (blue) result in 0.9 mm/year accumulation rate, while the west sabkha SB1 ages (orange) result in 1.7 mm/year. Locations of charcoal samples on trench logs are presented in Figs. 5 and 6. Radiocarbon age determinations in Table 1. (For interpretation of the references to colour in this figure legend, the reader is referred to the web version of this article.)

5. Discussion

5.1. Active faulting in Elat

Garfunkel et al. (1981) identified three types of active tectonic structures along the southern Arava Valley. First, active normal faults flank the western mountain range along the fronts of the mountains, but the faults are overlapped by the extensively dissected Garof fanglomerate of early Pleistocene age. We call this basin-bounding fault zone, the Elat Fault zone, and its main trace is seen on our seismic reflection profiles at CMP 262 (green fault in Line GI-2108; Figs. 4a and 9) and CMP 370 (green fault in Line SI-4047; Figs. 4b and 9). Second, within the Gulf of Aqaba/Elat, there are major bathymetric escarpments. These are the eastern and western normal faults, which bound the Elat deep marine basin along the 600 m isobath. Garfunkel et al. (1981) also mapped an active fault within the Elat Sabkha near the western border (east of the normal faults, but west of the main submarine fault escarpment). This location is near the offshore East Elat Fault (Hartman et al., 2014) and the fault we identified on seismic line GI-2108 at CMP 235 (Fig. 9). An aerial photo lineament to the north (Fig. 3) might be the northern extension of this feature. Further investigation of this structure is needed in order to recover the history of its seismic activity. Third, the active strike-slip fault that Garfunkel et al. (1981) called the Evrona (Avrona) fault zone, was mapped with prominent WNW- and ESE-facing fault scarps across a wide zone in the Avrona Sabkha where Holocene-age sabkha sediment are offset along pronounced scarps (Amit et al., 1999; Zilberman et al., 2005). Sparker seismic reflection data of the GAE shelf show that the Avrona Fault crosses the GAE continental shelf and projects onshore (Hartman et al., 2014).

Our interpretation of the seismic reflection data suggests that the Avrona Fault zone in the Elat Sabkha has been active in recent times. The offshore Avrona Fault is aligned with the fault mapped at CMP 125 of seismic reflection line G1–2108 and CMP 419 on SI-4047 (Fig. 9). In between these locations on a general trend of N20°E is evidence for active faulting in trench T3. We interpret this trend as the active main trace of the Avrona Fault through the Elat Sabkha. Subparallel faults that are also likely active or recently active are mapped to the east and west of the main Avrona Fault strand and have been labeled the West Avrona Fault and the East Avrona Fault.

Only the Avrona and East Avrona faults align with aerial photo lineaments. The surface trace of the Avrona Fault is likely characterized by *en echelon,* stepping fault strands within the Elat Sabkha. The fault in T3 trench does not correspond to the location of a lineament identified in this study. It is possible that some of the lineaments we mapped are controlled by and/or modified by the dominant south and southwest drainage of the Arava Valley.

Given the poor resolution of the seismic reflections at the top ~50 ms, it is difficult to definitively trace the fault to the surface. The interpretation of the fault at CMP 180 on GI-2108 (West Avrona Fault) may not be currently active as no offshore fault was found at this location or surface lineament identified. Seismic reflection data shown on seismic line W03a in Hartman et al. (2015) show mostly parallel reflectors to a depth of 70 ms without any evidence of faulting corresponding to CMP 180.

In the Elat Sabkha, we define a main through-going fault that has upward branching splays and fold deformation forming a positive flower structure. Other subparallel fault strands have likely recently been active and form a fault zone that is about 750 m wide. A similar pattern of multiple flower structures over a zone of about 1 km was imaged across the fault zone on seismic reflection data in the Avrona Sabkha (Shtivelman et al., 1998). Interpretation of ground penetrating radar data of the upper 25 m of sediment across the fault zone in the Avrona Sabkha suggests that faults splay upward into multiple fractures near the ground surface (Basson et al., 2002). Another seismic reflection survey in the central Arava Valley near a slight restraining bend in the DST (Haberland et al., 2007) showed a main through-going and continuous strike-slip fault. Multiple subparallel to anastomosing fault strands are found within a 100–300 m zone of the main fault. Tilting of strata caused by the interaction of the fault strands has created positive flower structure geometries.

Offshore geophysical surveys have identified a number of submarine faults in the northern Gulf of Aqaba (Makovsky et al., 2008; Tibor et al., 2010; Hartmann et al., 2014). The main offshore strike-slip fault, the Avrona Fault, clearly is youthful as it has a geomorphic expression on the seafloor and offsets the most recent sediment. The offshore Avrona Fault has been shown to have a Holocene average left-lateral, slip rate of 2.3–3.4 mm/yr based on offset coral reefs (Makovsky et al., 2008; Hartman et al., 2014). The Avrona Fault also has an apparent down-to-the-northwest normal slip component in the offshore that marks the edge of the so-called Ayla Horst block (Fig. 2). We see a dominant down-to-the-southwest component of subsidence on the seismic reflection profiles at CMP 444 (and line GI-2210). These data suggest that the eastern margin of the Elat Sabkha is controlled by left-oblique, normal slip. Strata that thicken toward the fault on the seismic reflection profile GI-2210 (Fig. 4) are interpreted as syntectonic deposition.

The most recent faulting on the Northern GAE is in an intermediate phase of evolution, where slip is partitioned onto marginal normal faults and strike-slip and oblique-slip intrabasinal faults (Hartman et al., 2014), while the activity and slip measurements across the faults imply that a major strike-slip fault, the Avrona Fault, occupies most of the Holocene left-lateral slip within the basin. Hartman et al. (2014) suggests a migration of the tectonic activity within the basin, as slip is carried from faults along the southeastern margin of the Northern GAE

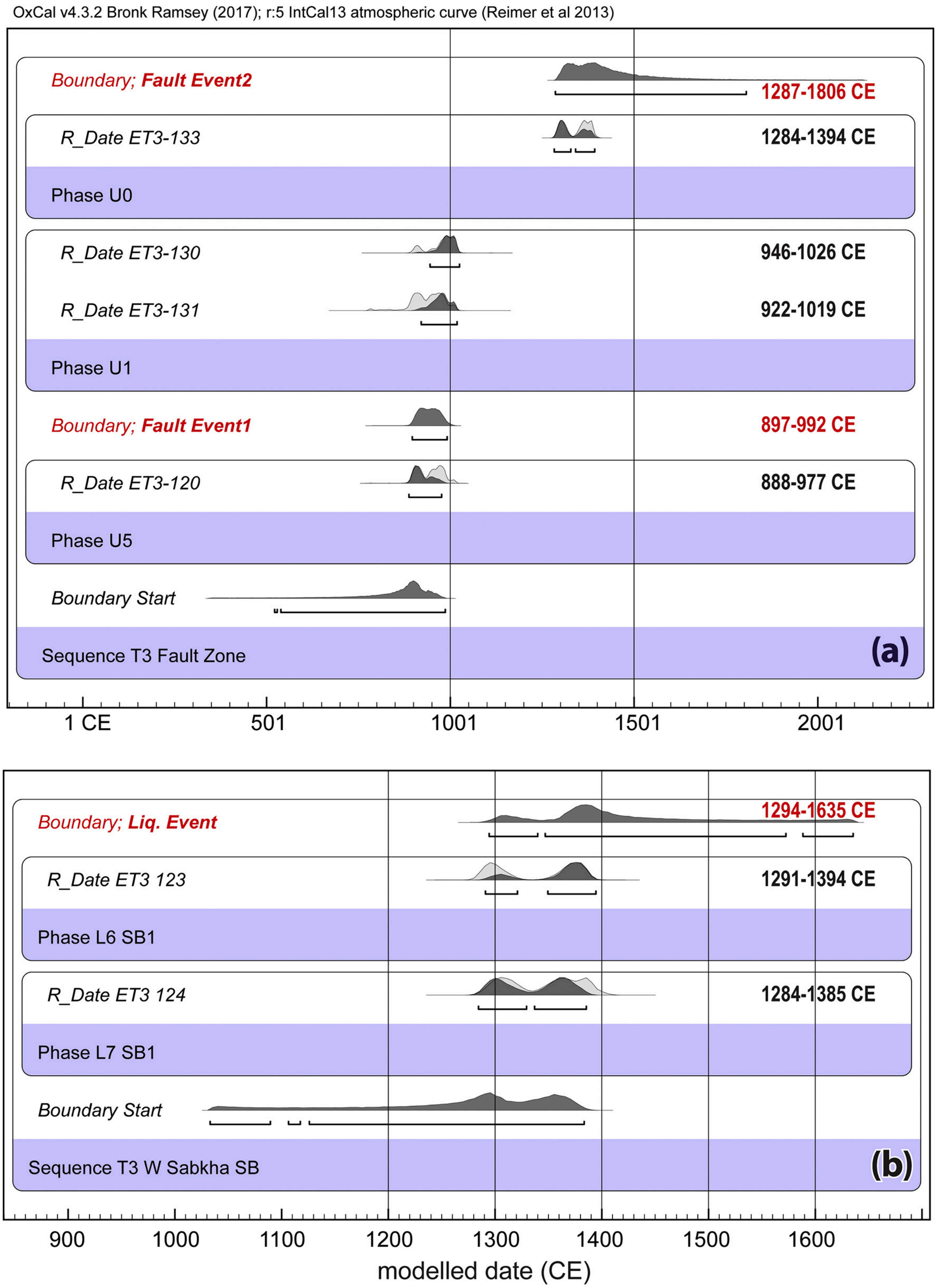

Fig. 8. Radiocarbon age models for the deformation and liquefaction events in trench T3 using OxCal software: (a) OxCal modeled age for liquefaction event using samples from stratigraphic units L6 and L7 from SB1 and the liquefied sand from SB2. (b) OxCal modeled age for faulting events E1 and E2 using samples from stratigraphic units U0, U1, U4 and U5 from the fault zone. Model calculated using OxCal 4.3.2 and IntCal13 calibration curve (Bronk Ramsey, 2017; Reimer et al., 2013).

to the northwestern margin. The offshore Avrona Fault may have localized slip from the two marginal faults into a single fault strand, which may in the next phase develop into a diagonal fault between the two marginal faults as previously suggested in basin evolution models along strike-slip faults (Marco, 2007; Schattner and Weinberger, 2008; Zhang et al., 1989).

Interpretation of aeromagnetic data across the Arava Valley show a continuous transform fault within a zone of several 100 m (ten Brink

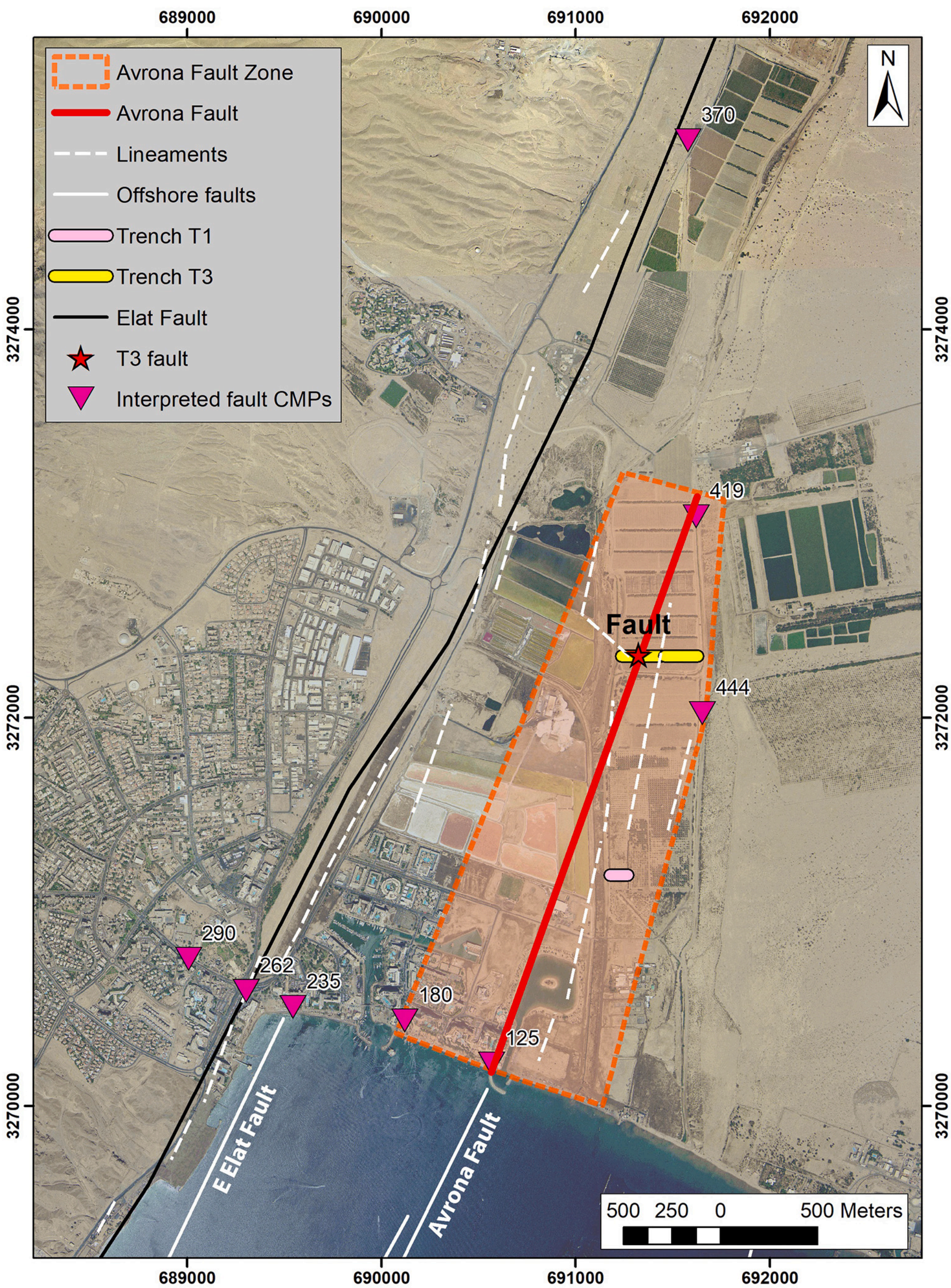

Fig. 9. The Avrona Fault, Avrona Fault Zone and active fault map based on the evidence for faulting presented in this study. The solid red line outlines the interpreted area with surface rupture evidence presented in this study from analysis of seismic reflection data (pink triangles) and the trench T3 fault zone (red star; location 34°58′29.86″E, 29°33′57.66"N). The area in dashed orange line is a suggested fault zone based on interpretation of our fault-potential lineaments presented in Fig. 3 (white dashed lines) and possible surface faulting deduced from the seismic reflection line GI-2108 between CMPs 125–180 (pink triangles). See legend for details. (For interpretation of the references to colour in this figure legend, the reader is referred to the web version of this article.)

et al., 2007). Ten Brink et al. (2007) show that the magnetic anomaly is very abrupt on the western side indicating that transform motion has been confined to its present position and eastward. Trapped basins on the east suggest that transform motion is either distributed to the east or that over time the Avrona Fault has migrated westward (ten Brink et al., 2007). Potential westward migration of strike slip is corroborated by Sparker seismic reflection data on the northern GAE shelf where Hartman et al. (2014) show that the Ayla and West Ayla faults located in the center of the GAE have become inactive in the Holocene and motion likely transferred to the Avrona Fault. This is also substantiated by the observation that the Holocene horizontal slip rate on the Avrona Fault has tripled since the Pleistocene (Hartman et al., 2014) from 0.7 ± 0.3 mm/yr in the late Pleistocene to between 2.3 and 3.4 mm/yr in the Holocene. This is probably related to the addition of slip from parallel faults. Faults east of the Ayla Horst (Ayla and Ayla East faults; Fig. 2) appear to be inactive. Hence, about 50–85% of the 4.7 mm/yr of the plate boundary motion appears to be concentrated on the Avrona Fault zone.

5.2. *Paleoearthquake surface rupture and liquefaction*

Haynes et al. (2006) infer from historical earthquake intensity data that major post-sixth century earthquakes probably occurred in the Wadi Araba and Dead Sea Fault in 634, 659/660, 873, 1068, 1212, 1293, 1458, 1546, and 1588 CE (Russell, 1985; Ben-Menahem, 1991; Ambraseys et al., 1994; Amiran et al., 1994; Guidoboni et al., 1994; Guidoboni and Comastri, 2005; Ambraseys, 2009). Klinger et al. (2015) narrow the largest well documented events of the southern DST after the eighth century to 1068, 1212, 1293, and 1458 CE. The surface rupture events, E1 and E2, that we document in the Elat Sabkha trench T3 appear to best correlate with the 1068 CE and 1458 CE historical earthquakes.

Klinger et al. (2015) radiocarbon dated ruptures at the Qatar site (Yotvata/Taba/Timna Sabkha), 30 km north of Elat and Aqaba, in the historical earthquakes of 1068 CE, 1212 CE, and 1458 CE, and two other earlier earthquakes in 746–757 CE and 363 CE. They suggest that the surface rupture of the 1068 CE earthquake terminated somewhere close to the Yotvata Sabkha and their Qatar trench site (Fig. 1b). Our data of surface rupture in the Elat Sabkha brings new evidence for southward continuation of the 1068 CE faulting, which was identified by Zilberman et al. (2005) in the Avrona Sabkha further north. We confirm the hypothesis by Klinger et al. (2015) about the southward continuation of the fault.

The rupture length of the 1068 CE earthquake fault can be constrained by the current study, documentation of rupture at the Avrona Sabkha (Zilberman et al., 2005), and the observations by Klinger et al. (2015). If we combine the 35 km of rupture onland from Qatar trench in the Yotvata Sabkha to trench T3 in Elat with the mapped offshore length of the fault 2 km further south from the coast (Hartman et al., 2014), a minimum of 37 km likely ruptured in the 1068 CE earthquake. Using the empirical relationship between fault rupture length and magnitude of Wells and Coppersmith (1994), we suggest a magnitude of M 6.6–7.1 for the 1068 CE earthquake. Historical accounts report massive destruction in the ancient Islamic city of Ayla in 1068 (Guidoboni and Comastri, 2005; Ambraseys, 2009). Compelling evidence for earthquake damage is confirmed by archaeological excavation of the Ayla site in Aqaba (Whitcomb, 1994). A reported possible tsunami in 1068 CE also supports a partial offshore rupture and/or seismically-induced submarine slump failures. Our results refute the location suggested by Ambraseys and Melville (1989) who located the 1068 CE event in NW Saudi-Arabia.

No earthquake rupture evidence was observed for the 1212 CE earthquake in the current study. Klinger et al. (2015) suggested that the rupture segment of the 1212 CE earthquake extends from the Qatar trench site south to the northern Gulf of Aqaba/Elat, thus to the T3 and T1 trench site. Klinger et al. (2015) report that this earthquake produced extensive damages to the city of Ayla and was widely felt in Egypt and reported north in the Wadi Araba (Ambraseys, 2009). A brecciated layer is associated to this event in the Dead Sea basin (Kagan et al., 2011), but no ground rupture related to this event was identified at the trench site of Qasr Tilah, located near the south boundary of the Dead Sea basin (Haynes et al., 2006). This leads us to suggest that either the 1212 CE faulting might have occurred elsewhere on another fault strand in the Elat Sabkha and not in the fault zone documented in trench T3, or possibly, the surface faulting did not extend as far south as Elat. Zilberman et al. (2005) suggest that the stronger earthquake of 1068 CE seems more likely to have caused the severe damage and surface rupture of the Avrona Sabkha area than the weaker 1212 CE earthquake. This supports an above assumption that the 1212 CE earthquake did not rupture the Avrona Fault. However, Guidoboni and Comastri (2005, p. 233-234) write that the primary source for this earthquake is Abu Shama from Damascus who wrote: “The most violent shock was at Aylat, on the coast.” This is the city of Aqaba. It is possible that the location of the earthquake rupture for the 1212 CE earthquake is a submarine segment of the fault in the northern Gulf of Aqaba/Elat. This could suggest that fine, cm-scale fracturing may be created by seismically induced ground motion rather than surface rupture at the Qatar site.

Paleoliquefaction in the T1 trench may be related to the 1212 CE earthquake. Fluidized sediments that are likely mobilized by seismic shaking are capped by a flat-lying thinly bedded to laminated deposit of clayey silt and very fine sand (Fig. 6c). This layer is radiocarbon dated to 1269–1389 CE and was deposited after an earthquake. Therefore, the T1 paleoliquefaction may be evidence for the 1212 CE earthquake or even the 1068 CE earthquake in the Elat Sabkha.

Klinger et al. (2015) suggests that the 1458 CE earthquake ruptured a section of the Wadi Araba fault located between their site and the southern tip of the Dead Sea, while the current study suggests that an event post-dating 1287 ruptured the surface at the T3 trench in Elat. Klinger et al. (2015) suggest that there is no mention of significant damage to Aqaba in this period, and therefore inferred that the earthquake ruptured to the north in the central Wadi Araba. Zilberman et al. (2005) also do not report surface ruptures of this event in the Avrona Sabkha. It is possible that our E2 surface rupture is the earthquake of 1588 CE that was felt in northwest Arabia, Ayla, and Cairo (Ambraseys, 2009). Ambraseys and Melville (1989) placed the epicenter of this event in northwest Arabia. Klinger et al. (2015) do not find evidence for the 1588 CE earthquake surface rupture in their study area. Given the poor age constraints on the upper limit of the timing of faulting, we are unable to differentiate between the historical earthquakes of 1458 CE and 1588 CE. Our paleoliquefaction sand blows (SB1 and SB2) suggest that this earthquake occurred after 1287 CE and possibly before 1550 CE if we use a sediment accumulation rate to calculate the age of burial of the feature. These data tend to support an interpretation of 1458 CE, but are inconclusive.

In summary, the paleoseismic data suggest: 1) a faulting event (E1) in 897–992 CE, 2) a liquefaction event sometime before 1269–1389 CE, which could be the same as E1 or a different event, 3) a faulting event (E2) after 1294 CE, and 4) a liquefaction event after 1337 CE and possibly before 1550 CE, which may have occurred at the same time as faulting event E2, or in a different earthquake.

Our data suggest that either the 1458 CE or 1588 CE ruptured the Avrona Fault in the Elat Sabkha. Our data suggest that no large event occurred along the Avrona segment in the past ~550 years following the 1458 CE earthquake or 430 years following the 1588 CE earthquake. Given either scenario, it has been a significant period of time since the Avrona Fault has experienced a surface rupturing earthquake. Using a slip rate of 4.7 mm/yr (Niemi et al., 2001) for the DST, an estimated 1.9–2.6 m of strain has already accrued.

6. Conclusions

Evidence for active faulting and recent earthquake history within the city of Elat along the southern Dead Sea Transform (DST) fault system shows the importance of combining all available data from onshore and offshore for investigating seismic hazard at coastal environments.

Along the eastern margin of the Elat Sabkha, seismic reflection data reveal that the main Avrona Fault is a continuous, through-going strike-slip fault that connects the location of the offshore fault on the GAE continental shelf, to the trench T3 site, and 3 km inland to the CMP 419 on the north-south oriented SI-4047 seismic line. This fault is active and the flower-structure geometry indicates that it is predominantly a strike-slip fault. Two additional faults in the Elat Sabkha west and east of the main strand and likely subparallel to it define a 750-m-wide fault zone. The West Avrona Fault is vertical and parallel or subparallel to the main strand. The East Avrona Fault may have left-oblique normal slip. The data indicate syntectonic deposition and growth strata thickening toward the southwest and into the offshore marine basin.

The first paleoseismic trenching within the boundaries of Elat city identified the location of the on-land Avrona active fault within the Elat Sabkha. Connecting it to the offshore mapped fault places the Avrona Fault along a N20°E trend and extending approximately 2.2 km inland from the shoreline. We conclude that this is a capable active fault, which underlies the Hotel District of Elat city.

Evidence for surface rupture in two earthquakes is observed in the Elat T3 Trench. Radiocarbon dating suggests the two faulting events may correlate to the 1068 CE and 1458 or 1588 CE (the first better supported by sediment accumulation rate). The time constraints prevent an unequivocal distinction between the earthquakes of 1458 CE and 1588 CE. Hence, a third earthquake rupture cannot be excluded.

No earthquake surface rupture was observed for the 1212 CE earthquake in the current study. However, fluidized strata radiocarbon dated to before 1269–1389 CE may be evidence for the 1212 CE earthquake. The Elat Sabkha has a potential for recovering records of past liquefaction events. Two sand blows mapped in trench T3 may have occurred at the same time as in the second faulting event (either 1458 CE or 1588 CE).

Our data suggest that a minimum of 37 km likely ruptured in the 1068 CE earthquake, which corresponds to an M 6.6–7.1 earthquake, and ~ 430–550 years of quiescence, entailing a significant accumulation of strain. Together these data indicate a high seismic hazard in the greater Elat-Aqaba region.

Supplementary data to this article can be found online at https://doi.org/10.1016/j.tecto.2020.228596.

Credit author statement

All authors share the credit of the manuscript.

Declaration of Competing Interest

None.

Acknowledgments

We thank Gal Hartman, Julie Bauer, Tomer Ketter, Lisa Coianiz, and Lana Ashqar for assistance in the field. The kind cooperation of the Kibbutz Eilot farmers, headed by Rafi Sa'ar, who have allowed us trenching in their fields, is also preciously appreciated. We thank Tectonophysics editor Kelin Wang, Christoph Grützner, and an anonymous reviewer for comments and suggestions that helped improve this manuscript. This work was funded by the USAID-Middle East Regional Cooperation (MERC) grant TA-MOU-08-M29-036.

References

Abueladas, A., 2014. Assessment of Seismic Hazards along the Northern Gulf of Aqaba: Interdisciplinary Doctoral Dissertation (Geosciences and Civil Engineering). Geosciences Dept., University of Missouri, Kansas City 250 p.

Abueladas, A., Niemi, T.M., Al-Zoubi, A., Tibor, G., Kanari, M., Ben-Avraham, Z., 2020. Liquefaction susceptibility maps for the Aqaba-Elat region with projections of future hazards with sea level rise. Q. J. Eng. Geol. Hydrogeol. https://doi.org/10.1144/qjegh2020-039. qjegh2020-039.

Allison, A.J., 2013. Paleoseismology and Archaeoseismology along the Southern Dead Sea Transform in Wadi'Arabah near the Municipality of Aqaba, Jordan. PhD Dissertation. Geosciences Dept., University of Missouri, Kansas City 254 p.

Ambraseys, N., 2009. Earthquakes in the Mediterranean and Middle East: A Multidisciplinary Study of Seismicity up to 1900. Cambridge University Press, Cambridge, UK.

Ambraseys, N.N., Melville, Cp, 1989. Evidence for intraplate earthquakes in northwest Arabia. Bull. Seismol. Soc. Am. 79, 1279–1281.

Ambraseys, N.N., Melville, C.P., Adams, R.D., 1994. The Seismicity of Egypt, Arabia and the Red Sea. Cambridge University Press.

Amiran, D.H.K., Arieh, E., Turcotte, T., 1994. Earthquakes in Israel and adjacent areas – macroseismic observations since 100 Bce. Isr. Explor. J. 44, 260–305.

Amit, R., Harrison, J.B.J., Enzel, Y., 1995. Use of soils and colluvial deposits in analyzing tectonic events—the southern Arava rift, Israel. Geomorphology 12, 91–107.

Amit, R., Harrison, J.B.J., Enzel, Y., Porat, N., 1996. Soils as a tool for estimating ages of Quaternary fault scarps in a hyperarid environment—the southern Arava valley, the Dead Sea Rift, Israel. Catena 28, 21–45.

Amit, R., Zilberman, E., Porat, N., Enzel, Y., 1999. Relief inversion in the Avrona Playa as evidence of Large-Magnitude Historical Earthquakes, Southern Arava Valley, Dead Sea Rift. Quat. Res. 52, 76–91. https://doi.org/10.1006/qres.1999.2050.

Amit, R., Zilberman, E., Enzel, Y., Porat, N., 2002. Paleoseismic evidence for time dependency of seismic response on a fault system in the southern Arava Valley, Dead Sea rift. Israel. Geol. Soc. Am. Bull. 114, 192–206. https://doi.org/10.1130/0016-7606(2002)114<0192:peftdo>2.0.co;2.

Avner, U., 1993. The history of the southern Negev and Elat in the light of new studies. In: Cohen, M., Shiler, E. (Eds.), Elat—Man, Sea and Desert. Ariel Press, pp. 113–184.

Basson, U., Ben-Avraham, Z., Garfunkel, Z., Lyakhovsky, V., 2002. Development of Recent Faulting in the Southern Dead Sea Rift According to GPR Imaging. Stephan Mueller Special Publication Series, 2https://doi.org/10.5194/smsps-2-35-2002.

Ben-Avraham, Z., 1985. Structural Framework of the Gulf of Elat (Aqaba), Northern Red Sea. J. Geophys. Res. 90, 703–726. https://doi.org/10.1029/JB090iB01p00703.

Ben-Avraham, Z., Tibor, G., 1993. The northern edge of the Gulf of Elat. Tectonophysics 226, 319–331. https://doi.org/10.1016/0040-1951(93)90125-4.

Ben-Avraham, Z., Almagor, G., Garfunkel, Z., 1979. Sediments and structure of the Gulf of Elat (Aqaba) – Northern Red Sea. Sediment. Geol. 23, 239–267. https://doi.org/10.1016/0037-0738(79)90016-2.

Ben-Menahem, A., 1991. Four thousand years of seismicity along the Dead Sea Rift. J. Geophys. Res. 96. https://doi.org/10.1029/91jb01936.

Dziewonski, A.M., Ekström, G., Salganik, M.P., 1997. Centroid-moment tensor solutions for October–December 1995. Phys. Earth Planet. Inter. 101, 1–12. https://doi.org/10.1016/S0031-9201(96)03199-8.

Enzel, Y., Amit, R., Porat, N., Zilberman, E., Harrison, B.J., 1996. Estimating the ages of fault scarps in the Arava, Israel. Tectonophysics 253, 305–317.

Frieslander, U., 2000. The Structure of the Dead Sea Transform Emphasizing the Arava, Using New Geophysical Data. PhD Dissertation. Hebrew University, Jerusalem.

Garfunkel, Z., 1970. The Tectonics of the Western Margins of the Southern Arava. PhD Dissertation. Hebrew University, Jerusalem.

Garfunkel, Z., 1981. Internal structure of the dead-sea leaky transform (rift) in relation to plate kinematics. Tectonophysics 80, 81–108.

Garfunkel, Z., Zak, I., Freund, R., 1981. Active faulting in the Dead Sea Rift. Tectonophysics 80, 1–26.

Gerson, R., Grossman, S., Amit, R., Greenbaum, N., 1993. Indicators of faulting events and periods of quiescence in desert alluvial fans. Earth Surf. Process. Landf. 18, 181–202.

Ginat, H., Enzel, Y., Avni, Y., 1998. Translocated Plio-Pleistocene drainage systems along the Arava fault of the Dead Sea transform. Tectonophysics 284, 151–160. https://doi.org/10.1016/s0040-1951(97)00165-0.

Goodman Tchernov, B., Katz, T., Shaked, Y., Qupty, N., Kanari, M., Niemi, T., Agnon, A., 2016. Offshore evidence for an undocumented Tsunami event in the 'Low Risk' Gulf of Aqaba-Eilat, Northern Red Sea. PLoS One 11 (1), e0145802. https://doi.org/10.1371/journal.pone.0145802.

Guidoboni, E., Comastri, A., 2005. Catalogue of Earthquakes and Tsunamis in the Mediterranean Area from the 11th to the 15th Century. Istituto Nazionale di Geofisica e Vulcanologia, Rome.

Guidoboni, E., Comastri, A., Traina, G., 1994. Catalogues of Ancient Earthquakes in the Mediterranean Area up to the 10th Century. Instituto Nazionale di Geofisica, Rome.

Haberland, C., Maercklin, N., Kesten, D., Ryberg, T., Janssen, C., Agnon, A., Weber, M., Schulze, A., Qabbani, I., El-Kelani, R., 2007. Shallow architecture of the Wadi Araba fault (Dead Sea Transform) from high-resolution seismic investigations. Tectonophysics 432 (1–4), 37–50. https://doi.org/10.1016/j.tecto.2006.12.006.

Hartman, G., 2012. Quaternary Evolution of a Transform Basin: The Northern Gulf of Elat/Aqaba. Dept. Geophys. Planet. Sci. Tel Aviv University, Tel Aviv.

Hartman, G., Niemi, T.M., Tibor, G., Ben-Avraham, Z., Al-Zoubi, A., Makovsky, Y., Akawwi, E., Abueladas, A.R., Al-Ruzouq, R., 2014. Quaternary tectonic evolution of the Northern Gulf of Elat/Aqaba along the Dead Sea Transform. J. Geophys. Res. Solid Earth 119 (12), 9183–9205. https://doi.org/10.1002/2013JB010879.

Hartman, G., Niemi, T.M., Ben-Avraham, Z., Tibor, G., Al-Zoubi, A., Sade, R.A., Hall, J.K., Akawi, E., Abueladas, A., Al-Ruzouq, R., Makovsky, Y., 2015. Distinct relict fringing reefs in the northern shelf of the Gulf of Elat/Aqaba: markers of quaternary eustatic and climatic episodes. Sedimentology 62, 516–540. https://doi.org/10.1111/sed.12179.

Haynes, J., Niemi, T., Atallah, M., 2006. Evidence for ground-rupturing earthquakes on the Northern Wadi Araba fault at the archaeological site of Qasr Tilah, Dead Sea Transform fault system. Jordan. J. Seismol. 10, 415–430. https://doi.org/10.1007/s10950-006-9028-9.

Hofstetter, A., 2003. Seismic observations of the 22/11/1995 Gulf of Aqaba earthquake sequence. Tectonophysics 369, 21–36.

Ibrahim, K.M., 1991. The Geology of Wadi Rahma, Map Sheet no. 3049 IV. a publication for the Ministry of Energy and Mineral Resources. Nat. Resour. Authority. Geol. Dir. Mapp. Div., Amman, Jordan.

Kagan, E., Stein, M., Agnon, A., Neumann, F., 2011. Intrabasin paleoearthquake and quiescence correlation of the late Holocene Dead Sea. J. Geophys. Res. Solid Earth 116 (B4). https://doi.org/10.1029/2010JB007452.

Klinger, Y., Avouac, J.P., Karaki, N.A., Dorbath, L., Bourles, D., Reyss, J.L., 2000. Slip rate on the Dead Sea transform fault in northern Araba valley (Jordan). Geophys. J. Int. 142, 755–768.

Klinger, Y., Le Béon, M., Al-Qaryouti, M., 2015. 5000 yr of paleoseismicity along the southern Dead Sea Fault. Geophys. J. Int. 202, 313–327.

Le Beon, M., Klinger, Y., Amrat, A.Q., Agnon, A., Dorbath, L., Baer, G., Ruegg, J.-C., Charade, O., Mayyas, O., 2008. Slip rate and locking depth from GPS profiles across the southern Dead Sea Transform. J. Geophys. Res. 113, B11403. https://doi.org/10.1029/2007jb005280.

Makovsky, Y., Wunch, A., Ariely, R., Shaked, Y., Rivlin, A., Shemesh, A., Ben Avraham, Z., Agnon, A., 2008. Quaternary transform kinematics constrained by sequence stratigraphy and submerged coastline features: the Gulf of Aqaba. Earth Planet. Sci. Lett. 271, 109–122.

Mansoor, N.M., Niemi, T.M., Misra, A., 2004. A GIS-based assessment of liquefaction potential of the City of Aqaba, Jordan. Environ. Eng. Geosci. 10 (4), 297–320. https://doi.org/10.2113/10.4.297.

Marco, S., 2007. Temporal variation in the geometry of a strike–slip fault zone: examples from the Dead Sea Transform. Tectonophysics 445, 186–199.

McCalpin, J.P., 2009. Paleoseismology, 2nd edn. .

Niemi, T.M., Zhang, H., Atallah, M., Harrison, J.B.J., 2001. Late Pleistocene and Holocene slip rate of the Northern Wadi Araba fault, Dead Sea Transform, Jordan. J. Seismol. 5, 449–474.

Ostrovsky, E., 2005. The G1 Geodetic-Geodynamic Network: Results of the G1 GPS Surveying Campaigns in1996/1997 and 2001/2002. (Geophysical Survey of Israel Technical Project Report).

Porat, N., Wintle, A.G., Amit, R., Enzel, Y., 1996. Late quaternary earthquake chronology from luminescence dating of colluvial and alluvial deposits of the Arava Valley, Israel. Quat. Res. 46, 107–117. https://doi.org/10.1006/qres.1996.0051.

Porat, N., Amit, R., Zilberman, E., Enzel, Y., 1997. Luminescence dating of fault-related

alluvial fan sediments in the southern Arava Valley, Israel. Quat. Sci. Rev. 16, 397–402. https://doi.org/10.1016/s0277-3791(96)00101-1.
Ramsey, C.B., 2017. Methods for summarizing radiocarbon datasets. Radiocarbon 59, 1809–1833.
Rashdan, M., 1988. The Regional Geology of the Aqaba-Wadi Araba Area. Bulletin 7, Geological Mapping Division, Geology Directorate, Natural Resources Authority, Jordan 87 pp.
Reimer, P.J., Bard, E., Bayliss, A., Beck, J.W., Blackwell, P.G., Ramsey, C.B., Buck, C.E., Cheng, H., Edwards, R.L., Friedrich, M., 2013. IntCal13 and Marine13 radiocarbon age calibration curves 0–50,000 years cal BP. Radiocarbon 55, 1869–1887.
Russell, K.W., 1985. The earthquake chronology of Palestine and Northwest Arabia from the 2nd through the mid-8th century AD. Bull. Am. Sch. Orient. Res. 260, 37–59.
Sade, A.R., Hall, J.K., Tibor, G., Niemi, T.M., Ben-Avraham, Z., Al-Zoubi, A.A., Hartman, G., Akawwi, E., Abueladas, A., Amit, G., 2008. Multibeam Bathymetry of the Northern Gulf of Aqaba/Elat. Poster at 1:20,000 scale.
Schattner, U., Weinberger, R., 2008. A mid-Pleistocene deformation transition in the Hula basin, northern Israel: implications for the tectonic evolution of the Dead Sea Fault. Geochem. Geophys. Geosyst. 9, Q07009. https://doi.org/10.1029/2007gc001937.
Shaked, Y., Agnon, A., Lazar, B., Marco, S., Avner, U., Stein, M., 2004. Large earthquakes kill coral reefs at the north-west Gulf of Aqaba. Terra Nova 16, 133–138. https://doi.org/10.1111/j.1365-3121.2004.00541.x.
Shaked, Y., Lazar, B., Marco, S., Stein, M., Agnon, A., 2012. Late Holocene events that shaped the shoreline at the northern Gulf of Aqaba recorded by a buried fossil reef. Isr. J. Earth Sci. 58, 355–368. https://doi.org/10.1560/IJES.58.3-4.355.
Shtivelman, V., Frieslander, U., Zilberman, E., Amit, R., 1998. Mapping shallow faults at the Evrona playa site using high-resolution reflection method. Geophysics 63, 1257–1264.
Sneh, A., Bartov, Y., Rosensaft, M., 1998. Geological Map of Israel 1:200,000. Geological Survey of Israel, Jerusalem.
Stuiver, M., Polach, H.A., 1977. Discussion reporting of 14 C Data. Radiocarbon 19 (3), 355–363. https://doi.org/10.1017/S0033822200003672.
Stuiver, M., Reimer, P.J., Reimer, R.W., 2019. CALIB 7.1. [WWW program].
ten Brink, U., Rybakov, M., Al-Zoubi, A., Rotstein, Y., 2007. Magnetic character of a large continental transform: An aeromagnetic survey of the Dead Sea Fault. Geochem. Geophys. Geosyst. 8 (7). https://doi.org/10.1029/2007GC001582.
ten Brink, U.S., Rybakov, M., Al Zoubi, A.S., Hassouneh, M., Frieslander, U., Batayneh, A.T., Goldschmidt, V., Daoud, M.N., Rotstein, Y., Hall, J.K., 1999. Anatomy of the Dead Sea transform: does it reflect continuous changes in plate motion? Geology 27, 887–890.
Tibor, G., Niemi, T.M., Ben-Avraham, Z., Al-Zoubi, A., Sade, R.A., Hall, J.K., Hartman, G., Akawi, E., Abueladas, A., Al-Ruzouq, R., 2010. Active tectonic morphology and submarine deformation of the northern Gulf of Eilat/Aqaba from analyses of multi-beam data. Geo-Mar. Lett. 30, 561–573. https://doi.org/10.1007/s00367-010-0194-y.
Tuttle, M.P., Hartleb, R., Wolf, L., Mayne, P.W., 2019. Paleoliquefaction studies and the evaluation of Seismic Hazard. Geosciences 9, 311.
Wdowinski, S., Bock, Y., Baer, G., Prawirodirdjo, L., Bechor, N., Naaman, S., Knafo, R., Forrai, Y., Melzer, Y., 2004. GPS measurements of current crustal movements along the Dead Sea Fault. J. Geophys. Res. 109. https://doi.org/10.1029/2003jb002640.
Wells, D.L., Coppersmith, K.J., 1994. New empirical relationships among magnitude, rupture length, rupture width, rupture area, and surface displacement. Bull. Seismol. Soc. Am. 84 (4), 974–1002.
Whitcomb, D., 1994. Ayla: Art and Industry in the Islamic Port of Aqaba. Special Publications, Oriental Institute, University of Chicago, Chicago, IL 32 p.
Wieler, N., Avni, A., Ginat, H., Rosensaft, M., 2017. Quaternary Map of the Eilat Region on a Scale of 10:000 with Explanatory Notes. Geological Survey of Israel Report No. GSI/37/2016, 16 pp. (in Hebrew, English abstract).
Wust, H., 1997. The November 22, 1995 Nuweiba Earthquake, Gulf of Elat (Aqaba): Postseismic Analysis of Failure Features and Seismic Hazard Implications. Geol. Surv. Israel. Report GSI/3/97.
Zak, I., Freund, R., 1966. Recent strike-slip movements along the Dead Sea rift. Isr. J. Earth-Sci. 15, 33–37.
Zhang, P., Burchfiel, B.C., Chen, S., Deng, Q., 1989. Extinction of pull-apart basins. Geology 17, 814–817. https://doi.org/10.1130/0091-7613(1989)017<0814:eopab>2.3.co;2.
Zilberman, E., Amit, R., Porat, N., Enzel, Y., Avner, U., 2005. Surface ruptures induced by the devastating 1068 AD earthquake in the southern Arava valley, Dead Sea Rift, Israel. Tectonophysics 408, 79–99. https://doi.org/10.1016/j.tecto.2005.05.030.